University of Siena – Department of Medical Biotechnologies

Doctorate in Genetics, Oncology and Clinical Medicine (GenOMeC)

XXXIV cycle (2018-2021)

Coordinator: Prof. Francesca Ariani

Deciphering the T-cell differentiation landscape in patients with Acute Myeloid Leukemia

Scientific disciplinary sector: MED/15 – Hematology

Tutor

Prof. Sara Galimberti

PhD Candidate

Francesco Mazziotta

Academic Year 2020/2021

Table of Contents

Abstract

The role of T cells in chemotherapy response and maintenance of remission in acute myeloid leukemia (AML) is not fully understood. In solid tumors and chronic infections, exhaustion is a multistep process ranging from less differentiated progenitor exhausted (Tpex) to intermediate and terminally exhausted T cells (Beltra et al. 2020). High frequencies of Tpex correlate with response to immune-checkpoint blockade in solid tumors (Miller et al. 2019). In AML, where the backbone of treatment is chemotherapy, the role of dysfunctional T-cell subsets has yet to be elucidated. In our study we used different cohorts of AML patients to study the immunologic T-cell landscape. Particularly, we performed an exploratory flow cytometry analysis on samples collected at baseline and at response assessment from patients treated with chemotherapy. Through high dimensional flow-cytometry analysis we identified a $CD8^+$ $CD28^+$ $PD1^+$ subset increased at baseline and after treatment in responder patients vs non-responders. To further investigate these results, we applied the same approach to analyze samples from a cohort of relapsed/refractory AML patients treated with high dose cytarabine (HIDAC) plus pembrolizumab. In these cohort, patients with a higher frequency of $CD8^+CD45RA^-CD27^{+/int}CD28^+PD1^+TCF1^+$ (progenitor-exhausted like) were more likely to respond to therapy. Next, we decided to better characterize the identified subset and study the relationships with the others $CD8^+$ subpopulations by using 5' VDJ single-cell RNA sequencing. Studying the different gene signatures in our dataset, we identified 5 main CD8+ clusters: Naive, Tpex, Effectors, Terminally exhausted 1 (Term_exh1) and Terminally exhausted 2 (Term_exh2). Comparing these subsets in responders and non-responders, Tpex were

greatly increased in responders compared to non-responders at both timepoints (baseline and response assessment). Conversely, Term_exh2 cells were more abundant in non-responders. Of note, the two most upregulated genes in Tpex were GZMK and IL-7R. Next, we measured the magnitude of clonal expansion in antigen-experienced $CD8^+$ T cells in responders and non responders. The most clonally expanded subsets were Tpex and Effectors in responders and Term_exh2 in non-responders revealing a strong relationship between abundance and clonal expansion of the $CD8^+$ T-cell subsets. Our scRNAseq results were then confirmed at the protein level with spectral flow-cytometry and reproduced by manual gating of the $GZMK^+CD127^+$ subset which was significantly enriched ($p < 0.01$) in responders vs non-responders. Notable, patients with a higher-than-median frequency of $GZMK^+CD127^+CD8^+$ T cells experienced significantly ($p<0.02$) prolonged overall survival after therapy. These findings show that improving our understanding of the immune microenvironment in AML is critical for the rational integration of novel treatment strategies that seek to increase the response rate and/or maintain remission. We identified $GZMK^+IL7R^+$ $CD8^+$ cells as a distinct entity in the early differentiated $CD8^+$ memory T cell pool that is clonally expanded and more abundant in responders compared to non-responders. This subset has a stem-like signature and may be associated with longer in vivo $CD8^+$ T cell persistence and long-term AML control. An in-depth functional characterization with in vitro experiments and in vivo mouse models is currently ongoing.

1. Introduction and background

1.1 Acute myeloid leukemia. State of the art.

Acute myeloid leukemia (AML) is the most common type of acute leukemia in adults, accounting for approximately 80% of cases. Despite therapeutic advancements over the last several years, the outcomes of AML patients remain poor with a 5-year overall survival (OS) of less than 30% (Liersch et al., 2014; Walter et al., 2010). Although up to 70% of AML patients achieve a complete remission (CR) after induction chemotherapy, the majority will ultimately relapse and die of their disease (Burnett et al., 2013). Long-term survival depends on several patient- and disease-related factors, including age, performance status (fitness for therapy), cytogenetic/molecular abnormalities, and the presence of measurable residual disease (MRD) after treatment (Grimwade et al., 1998; Döhner et al., 2017; Schuurhuis et al., 2018). Young patients and those with a favorable cytogenetics are most likely to achieve a CR. Still, even for patients who initially respond to chemotherapy, the problem of relapse persists. In patients who are treated with consolidation chemotherapy alone after achieving remission, the 5-year cumulative incidence of relapse ranges from 35% in those with favorable risk cytogenetics to 80% in those with unfavorable risk cytogenetics (Burnett et al., 2013). Since around two-third of AML patients do not experience durable remissions there is the need for different therapeutic approaches, especially in the setting of early relapsed/primary refractory AMLs. The use of allogeneic stem cell transplantation (alloSCT) significantly reduces the rates of AML relapse due to the graft-versus-leukemia effect provided by the infused alloreactive T cells (Weiden et al., 1981; Parmar et al., 2011). Owing to refinements in risk stratification

coupled with improved assessments of MRD it is now possible to identify all the eligible candidates for alloSCT early on. Furthermore, the development of novel and safer transplant platforms, and introduction of alternative stem cell sources, such as haploidentical donors or umbilical cord blood, for patients without a matched sibling or unrelated adult donor, resulted in a wider application of alloSCT to all patients in need, as nearly all eligible patients now have a potential donor (Kanakry et al., 2015). In recent years, the usage of reduced-intensity conditioning regimens ameliorated transplant toxicity and extended the survival benefit of alloSCT to older patients (Ringdén et al., 2019). The success of alloSCT indicates that alloreactive T cells can potentially eradicate chemoresistant clones. Despite these advances, a substantial proportion of AML patients does not experience long-term survival after alloSCT and is at high risk of disease recurrence. For this reason, novel strategies with the potential to reduce relapse risk are required.

1.2 Novel immunotherapeutic approaches and their limitations

In the last few decades, several immunotherapeutic approaches, including bispecific T-cell engagers (BiTEs), immune checkpoint blockade (ICB) and chimeric antigen receptor (CAR)-T cells have been developed for a plethora of malignancies and showed robust clinical responses. Building on these successes, the same strategies have been used to treat myeloid malignancies. Some approaches are still under investigation while others gave only modest results. In AML, one of the main biological barrier that limits the application of antigen-targeted approaches is the lack of a leukemia-specific antigen that is shared or expressed by the majority of AMLs. Generally, the optimal

target for T-cell based immunotherapies is an antigen highly expressed by tumor cells, while absent or expressed at low levels in healthy tissues (Daver et al., 2021). Leukemic blasts express several antigens (eg. CD34, CD117, CD33) that are also shared by healthy hematopoietic cells. Thus, the on-target off-tumor toxicity (or lack of selectivity) impairs the efficacy and increases the toxicity of any immune strategies aiming at those antigens (Qasim et al., 2019). Another obstacle for cell therapy approaches (CAR-T and adoptively transferred T cells) is the limited in-vivo expansion and persistence after the product infusion (Chapuis AG et al., 2012). CAR-T cells persistence is a key for long-term remissions and definitive cures (Maude SL et al., 2014). The mechanisms determining the difference in persistence between the constructs are still poorly understood and several efforts have been made to overcome this limitation. The predominant hypothesis to explain this phenomenon is the delicate balance between T cell activation and exhaustion: chronic antigen stimulation leads to persistent T cell activation and ultimately exhaustion (Youngblood et al., 2010; Wherry et al., 2015). Variation in the costimulatory domain of CAR-T (4-1BB instead of CD28) resulted in a more stem-like memory cell product and prolonged in-vivo persistence (Long et al., 2015). Lastly, immunosuppressive bone marrow (BM) microenvironment may affect the efficacy of the immunotherapeutic strategies aiming to activate T cells, such as BiTEs or ICB. Thus, a systematic profiling of different immune cells is critical to improve our understanding of the AML BM microenvironment and to overcome the obstacles associated with the different immunotherapeutic strategies .

1.3 Immunologic landscape in cancer

The impairment of the immunologic microenvironment is a key factor for development and maintenance of cancer. T cells play a central role in immune surveillance by targeting and eliminating tumor and infected cells. Chronic states of persistent antigen exposure force $CD8^+$ T cells towards exhaustion and immune tolerance. Often considered the main marker of exhaustion, PD-1 is an antigen expressed by various hematopoietic cells including T cells, B cells, natural killer (NK) cells and NK T (NKT) cells following their activation. PD-1 binds two ligands known as programmed cell death 1 ligand-1 (PD-L1) and PD-L2. PD-L1 is expressed in hematopoietic and non-hematopoietic cells while PD-L2 expression is restricted to professional antigen presenting cells (APCs) and a subset of B cells. In T cells, PD-1 expression is induced by T-cell receptor (TCR) signaling and upregulated by cytokines. In tumors, PD-1 remains at high levels and inhibits T cell function by its interaction with PD-L1 and PD-L2 (Sharpe et al, 2017). The advent of PD-1/PD-L1 pathway blockade therapeutics (ICB) introduced the idea of awakening from exhaustion $CD8^+$ T cells to reinvigorate the anti-tumor immune response. These developments in immunotherapy changed the treatment paradigm for many solid and several hematologic malignancies (Robert C *et al*, 2015; Larkin J *et al*, 2019; Ansell SM *et al*, 2015). However, most of the patients eventually relapse and/or become resistant. Further, responses to ICB are sometimes minor and short-lasting and not fully dependent on PD-1 inhibition. For this reason, recent studies have focused on exploring the T cell differentiation landscape and on defining the key factors involved in the process of

exhaustion. In general, following the initial activation of T cells heterogeneous epigenetic commitments may arise and follow different lineages of differentiation (Muroyama Y *et al 2021*) (Figure 1). In chronic states, the thymocyte selection-associated high mobility group box protein (TOX) is involved in the formation of effector and memory cells and is critical in coordinating the early epigenetic imprinting of T-cell exhaustion (Khan *et al.*, 2019). The downstream process involves several other factors whose expression defines different stages of exhaustion. Among these factors, T cell factor 1 (TCF-1) marks the early stage of the process and confers stem-like features to early exhausted $CD8^+$ T cells while preventing their differentiation into terminally exhausted cells. Interestingly, PD1-mediated inhibition of TCR signaling and T cell over-activation appears to limit the progression towards the late stages of exhaustion (Chen Z *et al.,* 2019; McLane LM *et al,* 2019). Hence, the co-expression of TCF1 and PD1 characterizes a group of tumor infiltrating lymphocytes (TILs) with stem-like features that are potentially responsible for the persistence of tumor specific T cells (Siddiqui I *et al,* 2019*)*. Due to their phenotypic and functional characteristics, $TCF1^+PD1^+CD8^+$ cells are termed Tpex. ICB unlocks Tpex population to differentiate into intermediate-exhausted proliferating cells with cytotoxic potential. This mechanism behind ICB activity is supported by studies showing that high percentages of $TCF1^+PD1^+$ TILs correlate with clinical responses to ICB. After their activation proliferating cells further differentiate into non proliferating terminally exhausted cells. Although intermediate-exhausted cells are capable of targeting and potentially clearing tumor cells, they are not

fully functional compared to their healthy counterpart. Upon antigen removal, Tpex can regain their phenotypical and transcriptional features of healthy memory T cells but maintain epigenetic circuits of exhaustion. This “epigenetic scar” of exhaustion persists invalidating T cells immunologic functions (Abdel-Hakeem MS *et al*, 2021). Recently Galletti *et al,* 2020, further characterized Tpex as $CCR7^{+}GZMK^{+}PD1^{+}TIGIT^{+}CD8^{+}$ cells in healthy individuals as well as cancer patients. This subset represents the first stage of exhaustion.

Beside T cell exhaustion, T cells in AML patients undergo senescence and have different gene signatures in responders versus non-responders to chemotherapy (Knaus et al, 2018). This T cell subset highly expresses killer cell lectin-like receptor subfamily G member 1 (KLRG1), B3GAT1 (encoding CD57), and other killer cell lectin-like and killer cell immunoglobulin-like receptor (KIR) genes. The distinction between T cell exhaustion and senescent is still confusing because of some overlapping characteristics. However, there are strong evidences suggesting that they are two different states regulated by different molecular mechanisms (Reiser, J. 2016; Akbar, A. 2011; Liu, X 2018). Consistently, recent reports suggest that senescence and exhaustion follow a different epigenetic commitment and that senescence cells may derive from short-lived effector cells (SLECs)(Figure 1) (Muroyama, Y. 2021).

Exhaustion and senescence are two disfunctional states in T cells responsible for immune escape and therapy resistance. Understanding

the mechanisms that generate and further develop these two subsets is critical for the development of effective therapeutic strategies in AML.

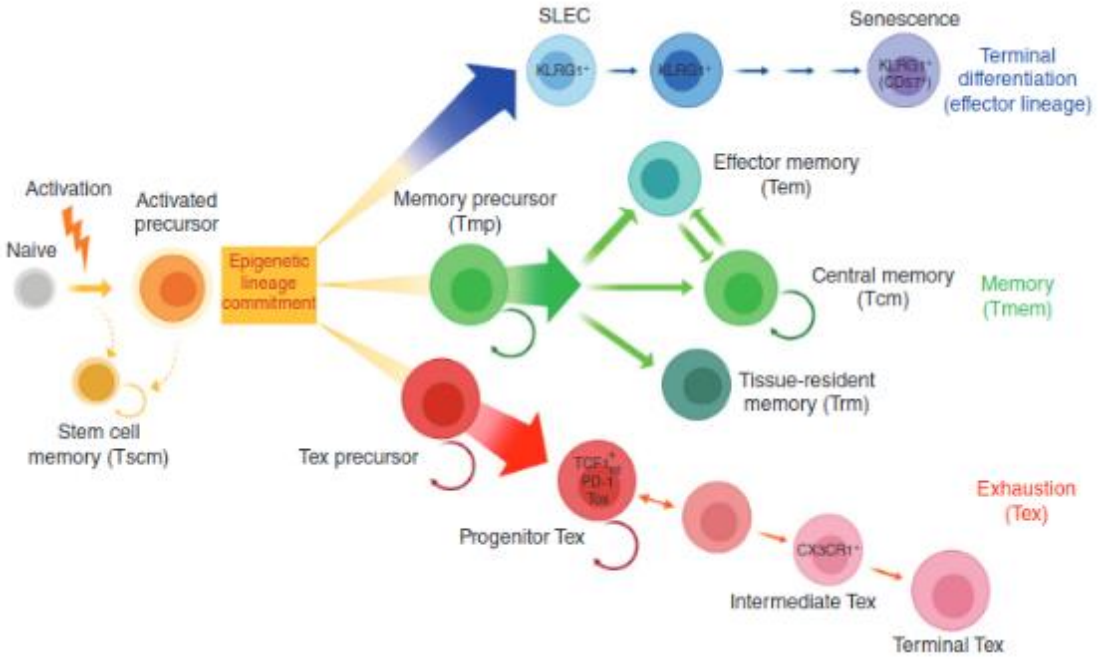

Figure 1: Lineages of CD8 T-cell differentiation upon activation (Muroyama Y et al. 2021)

1.4 Rationale for the study

In AML, T cells fail to eradicate leukemic blasts and become dysfunctional. Several mechanisms involving regulatory T cells (Tregs), M2 polarized macrophages, inhibitory T cell receptors, reactive oxygen species production and altered cytokine profiles may prevent proper T-cell activation and proliferation (Figure 2) (Vago *et al*, 2020; Szczepanski *et al*, 2009; Buggins *et al*, 2001; Al-Matary *et al*, 2016).

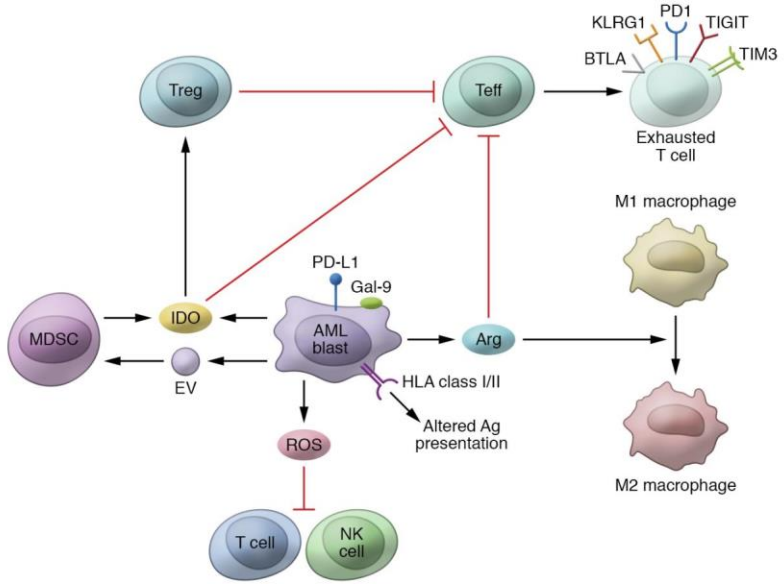

Figure 2: Immunotolerant microenvironment in acute myeloid leukemia

These complex cross-talks create an immune-tolerant niche that enables blast persistence. Yet, the potentially curative graft-versus-leukemia effect in patient treated with alloSCT marks the importance of engaging immunotherapeutic modalities in the treatment of AML. However, their applicability in AML is currently limited because of the major deficiencies in understanding the relevance of T cell states, including senescence and

exhaustion, in reactivating anti-leukemia immunity. A better understanding of the dynamics of T-cell differentiation in the AML BM microenvironment will not only inform the development of immunotherapeutic approaches to achieve long-term AML control but may also refine patient selection to those who are most likely to respond to different modalities, thus limiting unnecessary toxicities.

Thus, our goal was to elucidate the multistep differentiation process of T cells in AML at diagnosis and after treatment. To accomplish this goal, we performed flow-cytometry and single cell RNA sequencing (scRNA-seq) on BM samples collected from AML patients before and after chemotherapy, including healthy individuals as a biological control.

2. Materials and methods

2.1 Human subjects and specimens

BM mononuclear cells (BMMCs) were collected from AML patients and healthy volunteers, processed with Ficoll/Lymphoprep density centrifugation and cryopreserved. Treatment response was assessed using standard criteria (Döhner et al., 2017). The sample size was based on the number of available paired specimens from the same patients before and after induction chemotherapy. All the subjects signed the IRB approved consent form. Patient characteristics for the three cohorts used are described in table 1, 2, 3.

2.2 Flow cytometry (first chemotherapy cohort)

Antibodies were titrated to the optimal concentration as previously described. Surface staining was performed for 20 minutes at 37°C, while intracellular detection of cytokines was performed following fixation of cells with CytoFix/CytoPerm kit (BD Biosciences) according to the manufacturer's instructions and by incubating the cells with specific mAb cocktails for 20 minutes at room temperature. Serial BM samples from 33 newly diagnosed AML patients with well-annotated clinical data (10 complete responders (Res) and 6 nonresponders (NonRes) to chemotherapy) and 12 healthy donors (HDs) were analyzed. Flow cytometry was performed on a BD-LSRII (Becton Dickinson) and data were analyzed with BD FACSDiva software (Becton Dickinson) version 8.0.1. Antibodies used for analysis are listed in Table 4.

2.3 Flow cytometry (HiDAC + pembrolizumab cohort)

BMMCs were serially collected from AML patients (BM, n = 19) at baseline and at the time of response assessment after HiDAC plus pembrolizumab. Flow cytometry was performed on a BD-Fortessa (Becton Dickinson) provided with BD FACSDiva software (Becton Dickinson) version 8.0.1. Antibodies used for analysis are listed in Table 5.

2.4 Spectral flow cytometry (second chemotherapy cohort)

BMMCs were collected from AML patients (BM samples = 44) at baseline and at the time of response assessment after chemotherapy were acquired on a Cytek Northern Lights 3L 16V 14B 8R. Antibodies used for analysis are listed in Table 6.

2.5 High-dimensional flow cytometry analysis

Flow cytometry and spectral flow cytometry data were biexponentially transformed, compensated using single stained controls and preprocessed (aggregates and dead cell removal) in FlowJo V10 (TreeStar). Pre-gated $CD8^+$ T cells were then exported in R (version 4.0.2) for further analyses performed with a customized pipeline based on workflow (Nowicka et al., 2017). Specifically, $CD8^+$ T cells clusters were obtained using the FlowSOM algorithm and then visualized using the implementation of Uniform Manifold Approximation and Projection (UMAP) available in CATALYST R package. The different frequencies of the T cell subpopulations in CR (Res) and non-responders (NR) at the two timepoints (baseline and after treatment) were identified using the differential abundance analysis provided by the diffcyt R package (Weber et al., 2019).

2.6 Single cell RNA sequencing analysis

A DakoCytomation MoFlo (E1303A) (Beckman Coulter) was used to sort $CD3^+$ T cells. Gating strategy is shown in Figure 3. Cells were washed and resuspended in PBS + 0.04% BSA. The quantity and quality of the cells were assesed by Acridine Orange and Propidium iodide dye on a Cellometer Auto 2000 (Nexcelom). 16k cells with a viability higher than 85% were loaded on a 10x Chromium Controller based on 5' Chromium Single Cell V(D)J Reagent Kit manual (10x Genomics). After cell partitioning and GEM generation, reverse transcription was performed, and cDNA was pooled and cleaned up by beads. cDNA was further amplified for 13 cycles and cleaned up by SPRI beads (Beckman). The quality of cDNA was assessed by High Sensitivity D5000 Tapestation (Agilent Technologies Inc., California, USA and quantified by Qubit 2.0 DNA HS assay (ThermoFisher, Massachusetts, USA). T cell receptor (TCR) target enrichment, 5' Gene expression library, and TCR library was carried out according to 5' Chromium Single Cell V(D)J Reagent Kit manual (10x Genomics). Equimolar pooling of libraries was performed based on QC values and sequenced on an Illumina® NovaSeq (Illumina, California, USA) with a read length configuration of 150 PE for 600 M PE reads per sample (300M in each direction). The 10x genomics software Cell Ranger (version 4.0) was used to process the raw data FASTQ files with default parameters. The EmptyDrops method (Lun et al., 2019) was used to identify cells with low RNA contents. The "count" function was used to perform alignment, filtering, barcode counting, and UMI counting. This function uses the Chromium cellular barcodes to generate feature-barcode matrices,

determine clusters, and perform gene expression analysis. The "vdj" function was used to perform sequence assembly and paired clonotype calling for each cell. This function uses the Chromium cellular barcodes and UMIs to assemble V(D)J transcripts per cell. GRCh38 and GRCh38.p12 gtf were used as reference genome and annotation gtf file. Cellranger VDJ calling generates an output named as "filtered_contig_annotations.csv" for each sample. In this file, the CDR3 amino acid and nucleotide sequences for single cells were listed by cell barcodes.

The filtered feature matrices generated by the CellRanger pipeline were used for downstream quality control (QC) and analyses. Doublet cells filtering was performed on each sample using the *scds* package (Bais & Kostka, 2020). *scater* R package was used for QC and filtering (McCarthy et al., 2017). Genes undetected across all the cells were removed. Cells with feature counts, percentage of mitochondrial genes and number of expressed features beyond 2.5 median absolute deviations of the median were filtered out. Finally, we retained features with a count greater than 1 in at least 20 cells for downstream analysis. Next, *Seurat (Stuart et al., 2019)* (Butler et al., 2018) v4.0 was used for integration, clustering and dimension reduction. Integration and clustering were performed using the 2000 most highly variable genes for integration and clustering. Clustering and dimension reduction were computed using the first 20 principal components. Differential gene expression was performed using the *FindMarkers* function from Seurat. Cell trajectory inference was computed using *Silingshot* R package (v1.99.15) and using the *TradeSeq* R package (v1.7.02) for the differential gene expression along the trajectories. The function *earlyDETest* from *TradeSeq* was used to test differential gene expression at specific

pseudotime values. TCR analysis was performed using the *scRepertoire* R package (v0.99.3) (Borcherding et al., 2020). Weapplied the function c*lonalOverlay* using default settings to generate an overlay of the position of most clonally expanded cells projected onto UMAP.

2.7 Overall survival estimate in TCGA

Kaplan-Meier estimate of OS in TCGA AML cases stratified by CD52 expression (median split). The Gene Expression Profiling Interactive Analysis portal (http://gepia2.cancer-pku.cn/#survival) was used to access and analyze the data.

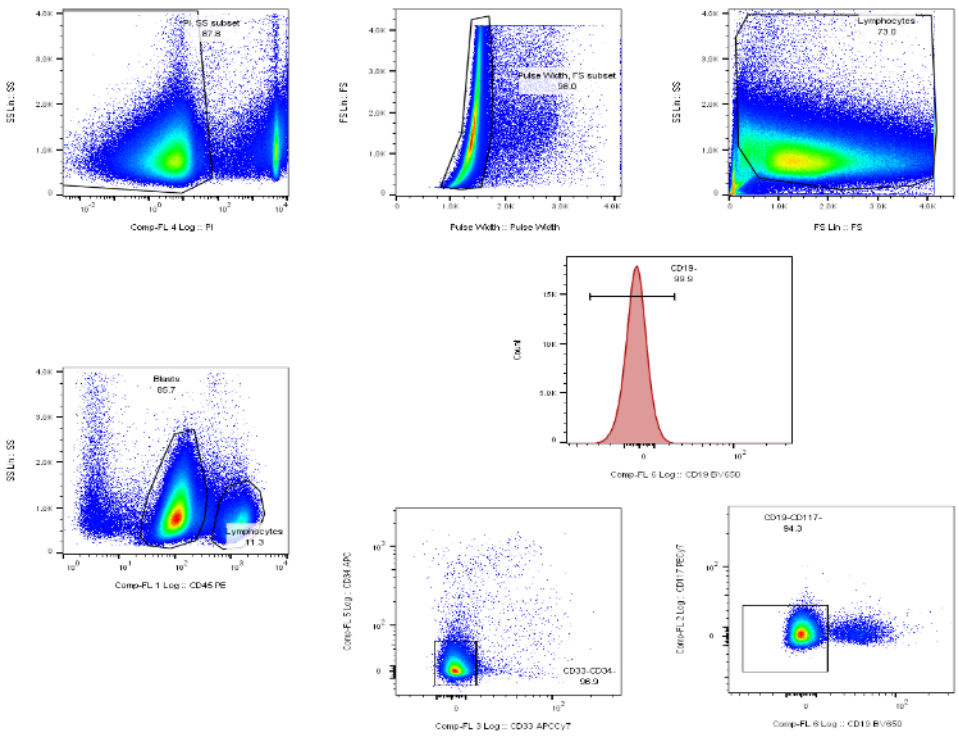

Figure 3: Sorting strategy used to sort CD3+ T cells

3. Results

3.1 A subset of PD1$^+$CD28$^+$ CD8$^+$ T cells correlate with complete response in AML patients undergoing chemotherapy

To study the complex immunologic landscape of AML, we applied high-dimensional analysis to flow data presented in Knaus HA *et al,* obtained through a 12-color panel. The heterogeneity of T cell states hampers the identification of cell subsets of interest via visual inspection of scatter plots displaying individual cells' fluorescence intensities. To avoid user bias and reduce the complexity of the data, we performed unsupervised clustering for cell subpopulations and uniform manifold approximation and projection (UMAP) for dimensionality reduction. This approach integrates markers at a single-cell level and provides insight into the true complexity of their high dimensional relationships. We analyzed BM CD8$^+$ T cells from AML patients (n = 16, 10 Res and 6 NonRes) at baseline and post-chemotherapy to define their state of differentiation, activation, and co-inhibitory molecule expression. The unsupervised clustering revealed 4 different CD8$^+$ cell states including naive (CCR7$^+$CD45RA$^+$CD27$^+$CD28$^+$), activated effectors (KLRG1$^+$CD160$^+$CD56$^+$), terminally differentiated/senescent (Temra/Sen) (CD45RA$^+$CD57$^+$KLRG1$^+$) and PD1$^+$CD28$^+$ cells (Fig. 4A). Visualization via UMAP revealed a different distribution of CD8$^+$ differentiation landscape in Res compared to NonRes (Fig. 4B). Specifically, NonRes patients had less naive and PD1$^+$CD28$^+$CD8$^+$ cells at both timepoints compared to the other subgroup. Similarly, Jansen CS *et al.*, 2019 recently identified an intra-tumoral TIM3$^-$PD1$^+$CD28$^+$ CD8$^+$ subset with stem-like features that can give rise to more terminally differentiated cells. A similar

subpopulation expressing PD1 and other "stem_like" markers has been described and referred as Tpex (Siddiqui *et al.*, 2019; Miller *et al.*, 2019). High percentages of Tpex pre-treatment, among exhausted $CD8^+$ tumor infiltrating lymphocytes, correlate with response to PD-1/PD-L1 pathway blockade in melanoma (Miller *et al.*, 2019).

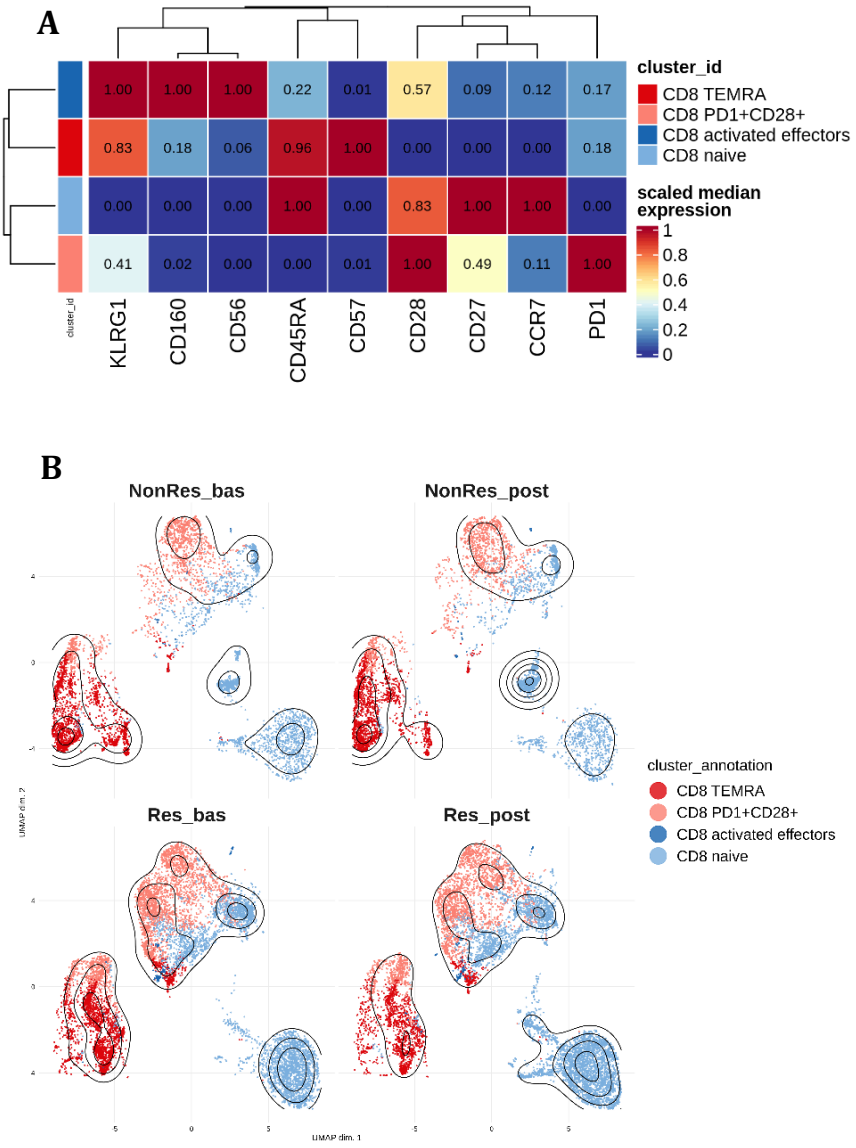

Figure 4:$CD8^+$ $PD1^+CD28^+$ and activated effectors cells are increased at baseline in patients who are more likely to respond to chemotherapy(A) Heatmap showing the 0-1 scaled MFI values of 9 markers over the four CD8+ BM subsets from all the samples (6 NonRes, 10 Res). The median marker expression identifies the markers that drive each cell subset. Each CD8+ subpopulation is colored according to the cluster identified using the FlowSOM algorithm. (B) UMAP visualization overlaid with contour plots (kernel density estimation) of the four CD8+ BM subpopulations in all the AML patients (NonRes, n = 6, Res, n = 10), at baseline and after therapy. Each CD8+ subpopulation is colored according to the cluster identified using the FlowSOM algorithm.

3.2 Progenitor exhausted CD8+ T cells are increased in AML patients who are more likely to respond to chemotherapy plus checkpoint inhibitors

We hypothesized that treatment with immune checkpoint inhibitors (ICB) likely influences T-cell exhaustion dynamics in AML. To understand whether $CD28^{+}PD1^{+}$ $CD8^{+}$ progenitor-exhausted-like T cells are associated with a better outcome in AMLs treated with ICB, we interrogated changes in T-cell states in patients enrolled in an open-label, single-arm, phase II study of high dose cytarabine (HiDAC) followed by pembrolizumab in relapsed/refractory (R/R) AML conducted at two institutions, the University of North Carolina, Lineberger Comprehensive Cancer and the Johns Hopkins Hospital, Sidney Kimmel Comprehensive Cancer Center (clinicaltrials.gov identifier NCT02768792). We performed flow-cytometry analyses on patient-derived BM samples (n = 19, 8 Res and 11 NonRes) aiming at the identification of biomarkers that were predictive of response to HiDAC/pembrolizumab. We detected 8 different clusters (Fig. 5A, B) with a significantly higher frequency of senescent T cells at baseline in NonRes (Fig. 5C). Interestingly, Res had significant increased frequency of $CD8^{+}$ T cells expressing CD27, CD28, PD-1, TIGIT, and lacking expression of Tim-3 and CD57 at baseline. This Tpex-like phenotype was consistent with our previous flow-cytometry findings in patients treated with conventional chemotherapy. Additional analysis using manual gating strategy involving the intracellular marker TCF-1 confirmed that there was a statistically significant increase in pre-treatment $CD8^{+}CD45RA^{-}$ $CD27^{+/int}CD28^{+}PD1^{+}TCF1^{+}$ T cells in patients who achieved Res compared to NonRes (Fig. 6). Taken together, these data identify a subset of progenitor

exhausted T cells within the AML microenvironment that may differentiate into effector-like CD8+ T cells and target tumor cells upon treatment with ICB (Beltra *et al.*, 2020).

A

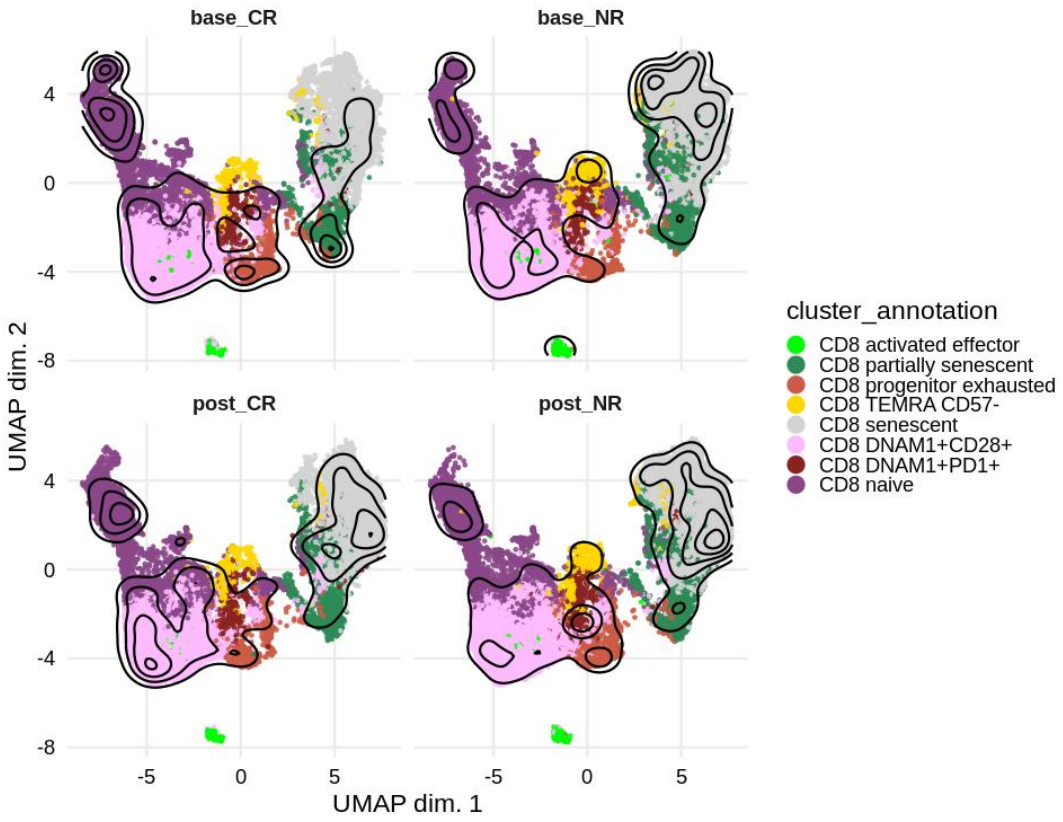

B

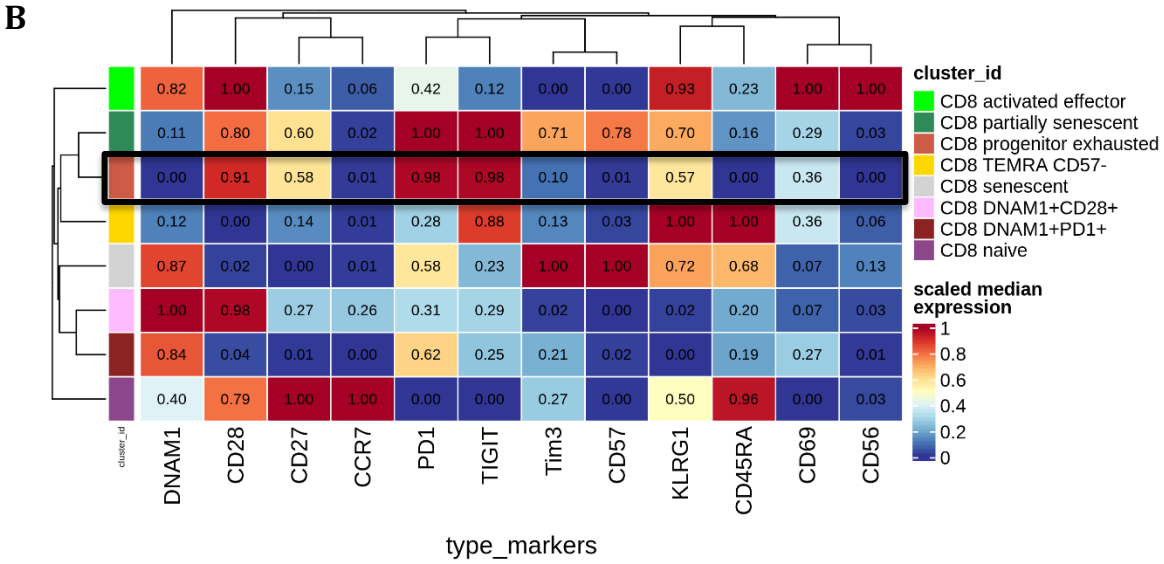

C

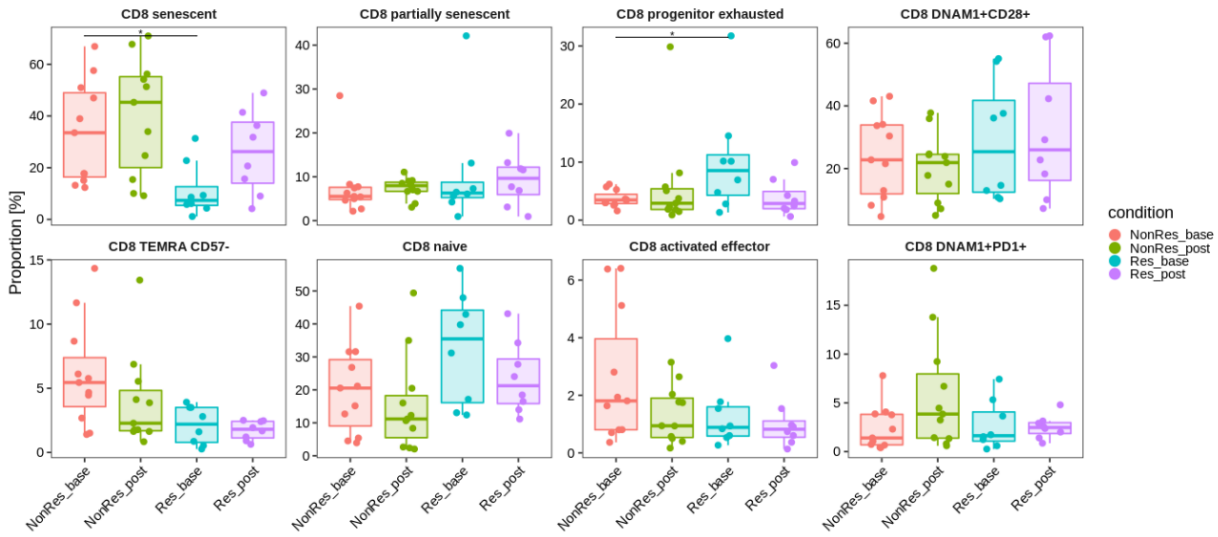

Figure 5: Immune biomarkers associated with response in patients treated with HiDAC + Pembrolizumab: Tpex are increased in patients who are more likely to respond

(A) UMAP visualization overlaid with contour plots (kernel density estimation) of the eight CD8⁺ BM subpopulations in non-responders (NonRes, n = 11) and complete responders (Res, n = 8), at baseline (Res_bas, NonRes_bas) or after therapy (Res_post, NonRes_post). Each CD8⁺ subpopulation is colored according to the cluster identified using the FlowSOM algorithm. (B) Heatmap showing the 0-1 scaled MFI values of 12 markers over the eight CD8⁺ BM subsets from all the samples (NonRes = 11, Res = 8, both timepoints). The median marker expression identifies the markers that drive each cell subset. Each CD8⁺ subpopulation is colored according to the cluster identified using the FlowSOM algorithm. (C) Boxplots showing the relative abundance of BM CD8⁺ subpopulations in NonRes and Res patients at baseline and post-treatment. Horizontal bars indicate median values. Asterisks indicate adjusted p-values (*padj< 0.05).

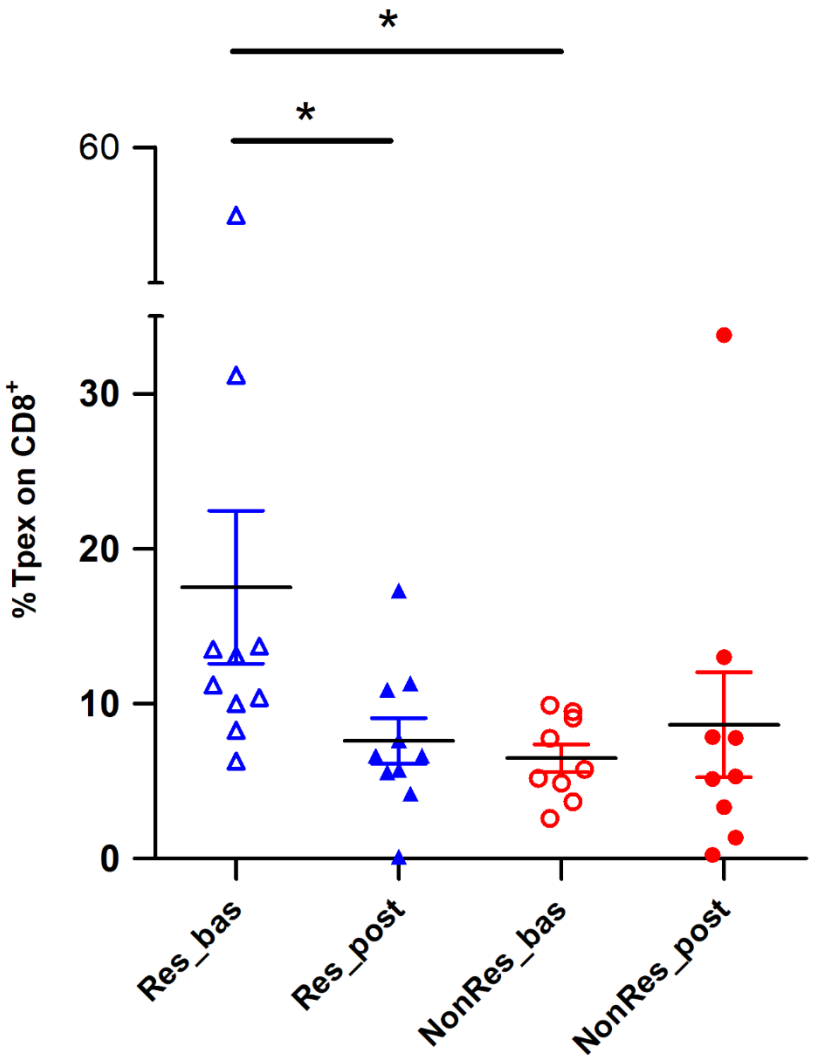

Figure 6: Frequency of BM CD8+CD45RA-CD27+/intCD28+PD1+TCF1+ T cells in patients who achieved CR compared to NRs at baseline and at response assessment (*p< 0.05).

3.3 Single cell RNA sequencing identifies a subpopulation of CD8$^+$ GZMK$^+$IL7R$^+$ progenitor exhausted cells that correlates with response in AML patients undergoing chemotherapy-only treatment

Although the results obtained in patients treated with ICB are promising, the backbone of treatment in AML remains chemotherapy. However, little is known about the T-cell differentiation landscape in AML patients

undergoing chemotherapy. Therefore, to validate our results and better characterize the T-cell landscape in AML we performed single-cell RNA sequencing (5' VDJ scRNA-seq; 10x Genomics Platform) on BM samples obtained from AML patients ($n = 5$; 3 Res, 2 NonRes) at baseline (base) and after chemotherapy (post) and 2 HDs. Preliminary results on whole BM and in silico analyses performed on published data (Dufva *et al*, 2020) revealed that the number of T cells was not sufficient to distinguish the different T cell subsets of interest. This technical issue is related to the relative predominance of the myeloid subpopulations in AML. Then we developed a sorting strategy to positively enrich BM $CD3^+$ T cells while eliminating myeloid cells, B cells and stroma (Fig. 3). This was accomplished by using a dumping channel (CD33, CD34, CD117, CD19) and sorting highly enriched but "untouched" $CD45^+$ fraction of 95% pure T cells sufficient for subsequent downstream scRNAseq analysis. With this strategy we obtained an average four-fold increase of T cells per sample (Fig. 7).

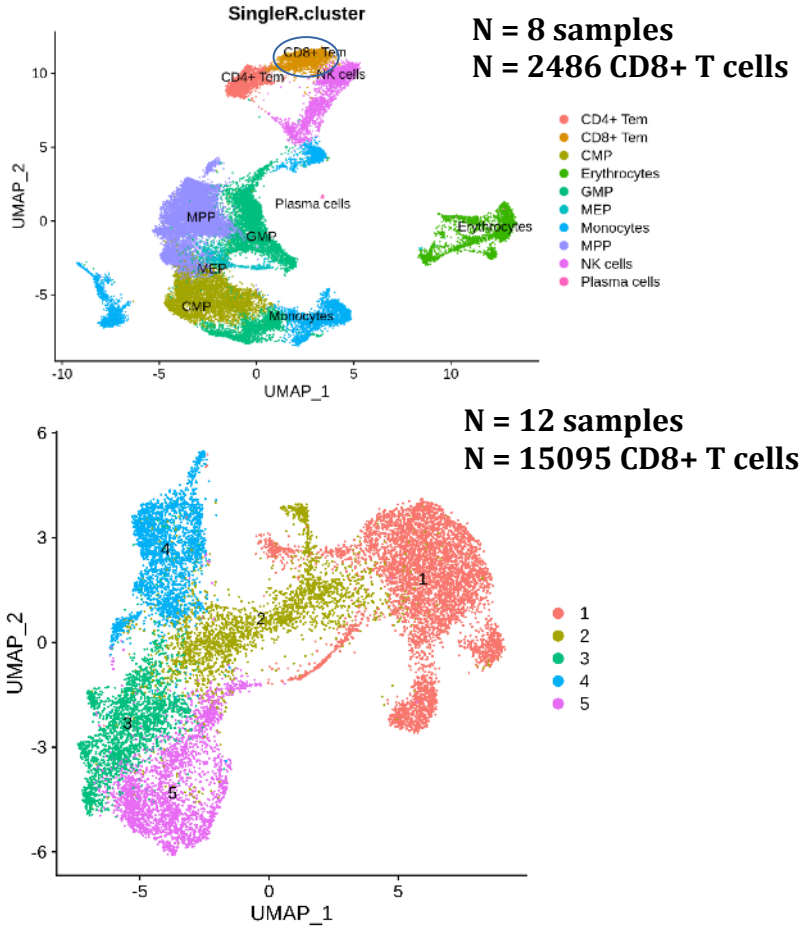

Figure 7: Comparison of CD8+ T-cell scRNAseq data obtained from whole bone marrow (Dufva et al. Cancer Cell 2020) and CD3+ sorted cells

For Res and NonRes samples, matched scTCR-seq information was also collected. After preprocessing and computational sub-setting of the $CD8^+$ T-cell subtypes, we collected data on 15095 $CD8^+$ T cells. We used already published (Szabo PA *et al,* 2019; Pace L *et al*. 2018; Miller BC *et al,* 2019) and customized gene signatures mapped in two dimensions via UMAP (Fig. 8) to define the identities of the clusters annotated as naive, Tpex, Effectors, Term_exh1 and Term_exh2 (Fig. 9). Of note, the two most differentially expressed genes in Tpex compared to all the other clusters were GZMK and interleukin (IL)-7 receptor (IL-7R), also known as CD127 (data not shown).

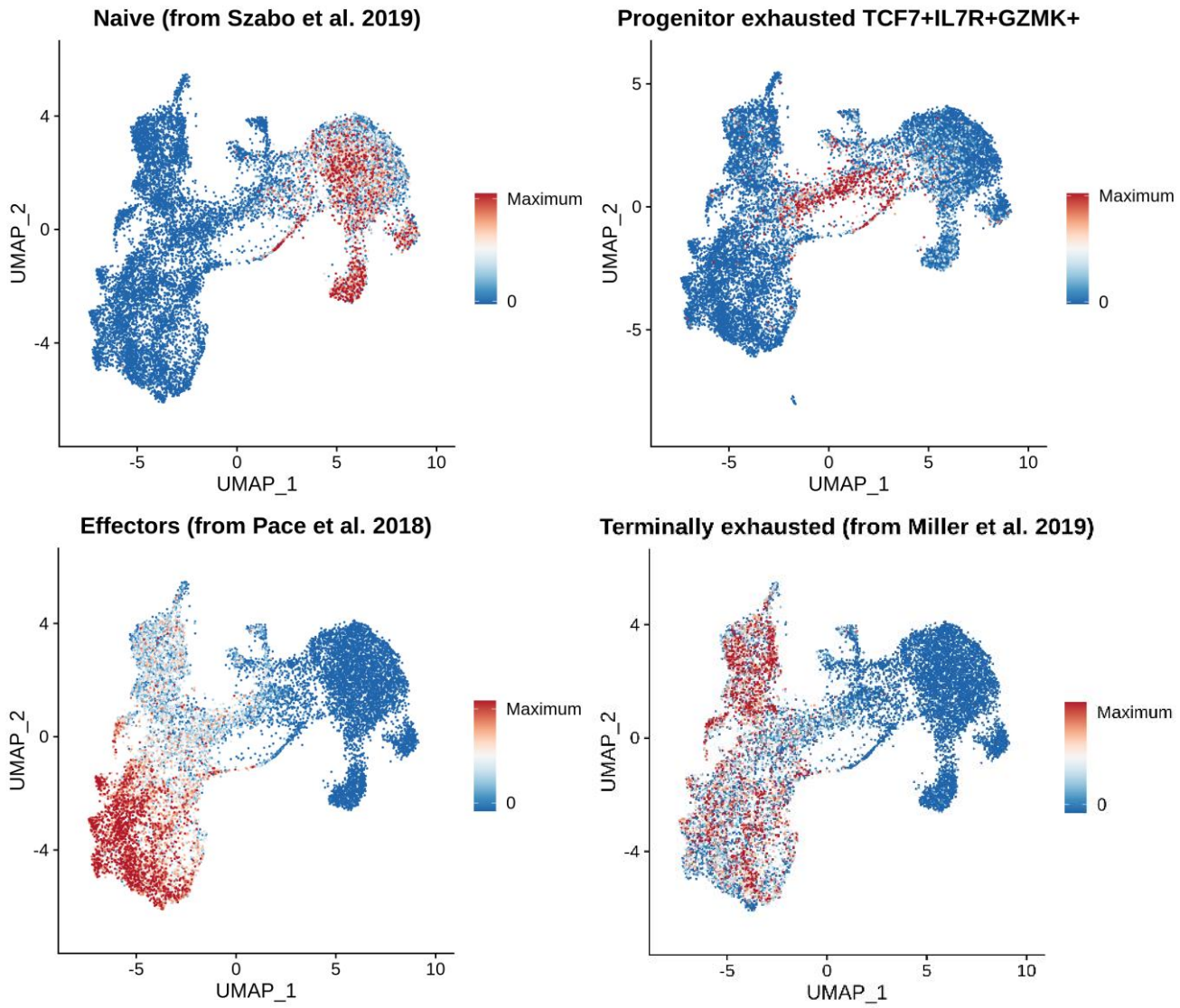

Figure 8: Projection of selected gene signatures and gene markers (GZMK, IL7R) identifying the different T cell states

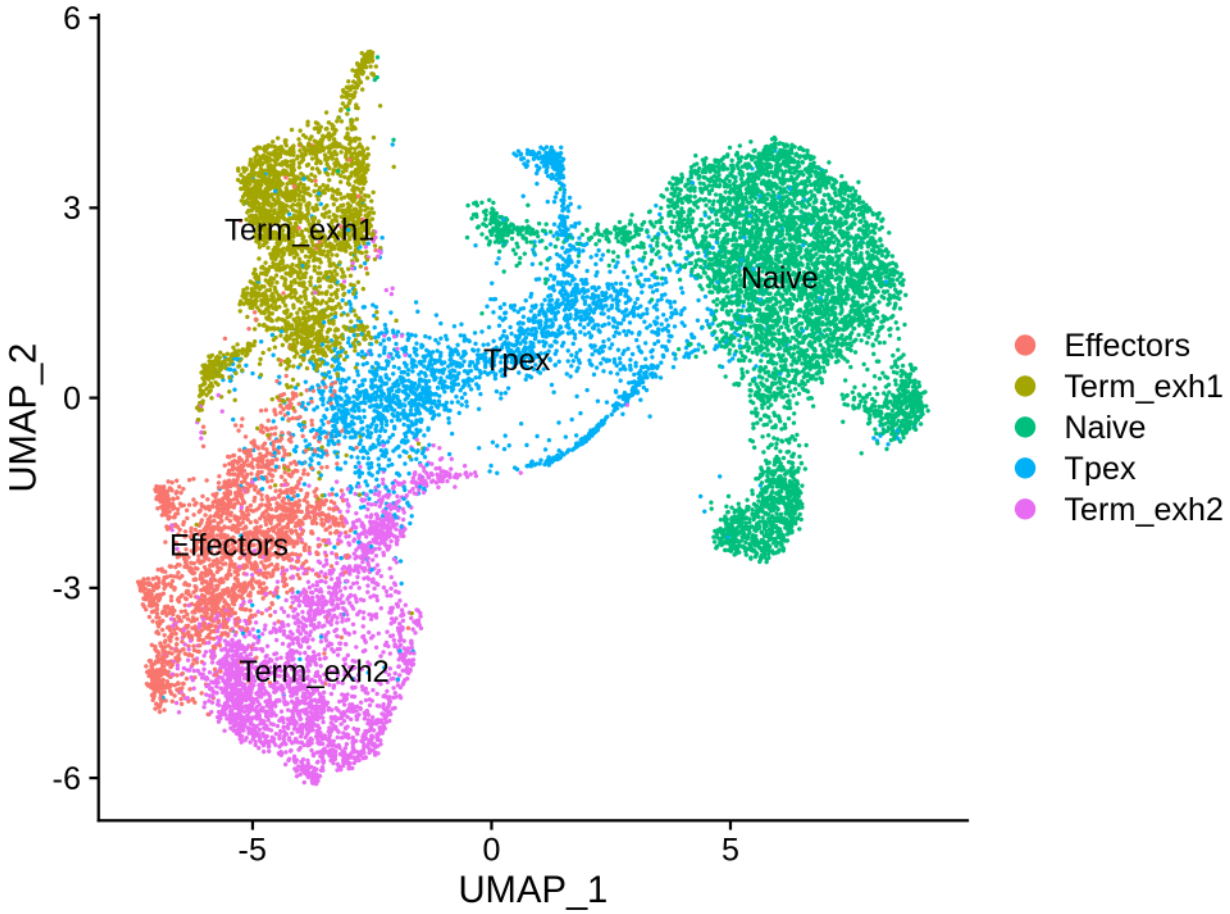

Figure 9: Unsupervised clustering of scRNAseq identified four main clusters: Tnaive, Tpex, Effectors, Term_exh1, Term_exh2

Next, we sought to understand if there was a difference in terms of clusters' abundancies across the three conditions (Res, NonRes, HD). Overall, the distribution of the $CD8^{+}$ states was similar in Res and HDs (Fig. 10A). Interestingly, Res samples had an increased frequency of Tpex and Effectors compared to NonRes (Fig. 10A-B). Conversely, NonRes presented with a notable increase of Term_exh2 compared to Res and HDs (Fig. 10A-B). These differences in clusters' frequencies were present at both baseline and post-chemotherapy (Fig. 11).

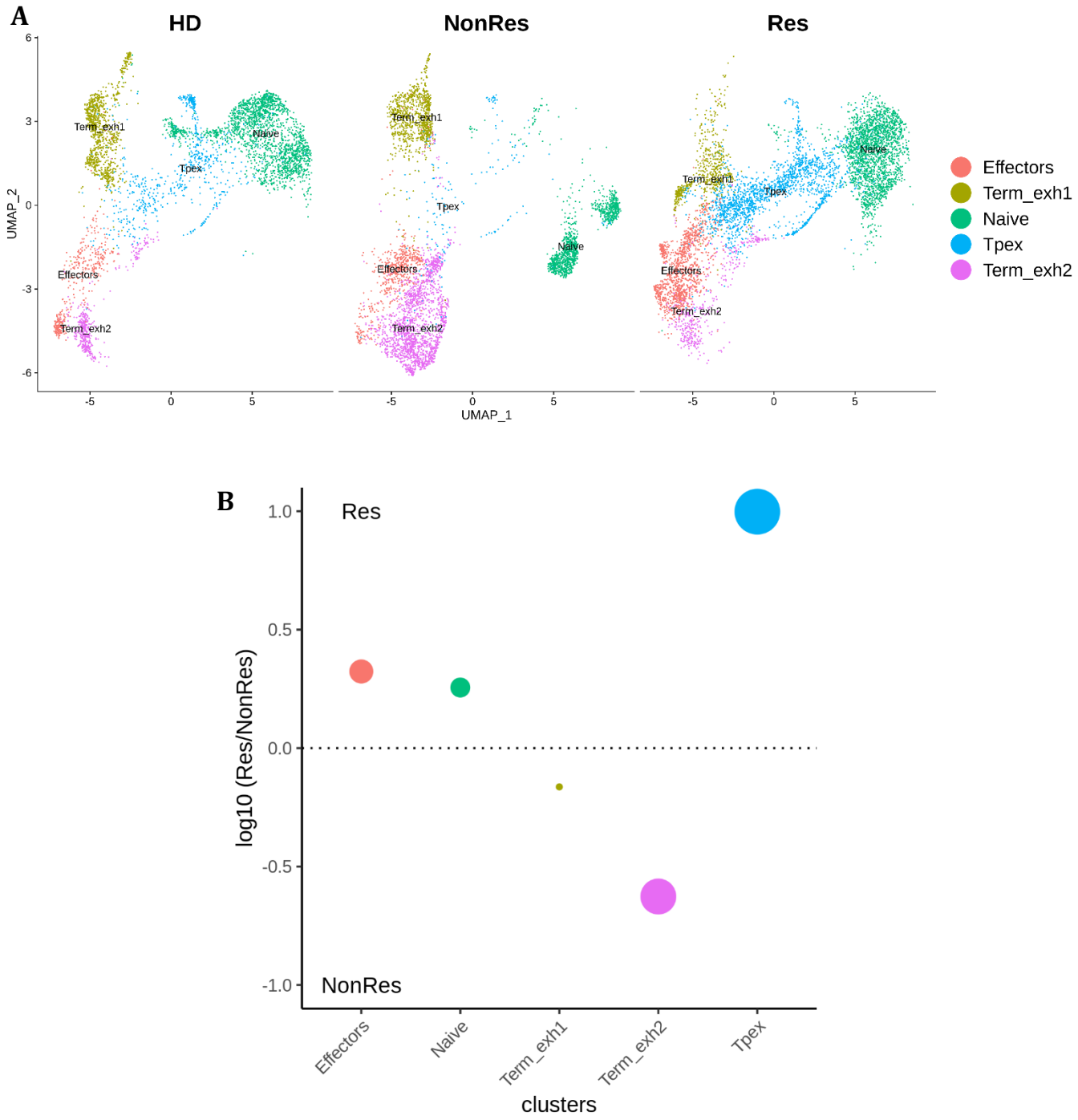

Figure 10: Tpex and effectors are increased in Res vs NonRes; Term_exh2 are increased in NonRes vs Res

(A) UMAP split by response to chemotherapy showing in 2 dimensions the distribution of the five identified BM CD8⁺ subsets across the three conditions (Res, NonRes, HD). (B) Summary dot plot showing relative frequency of BM CD8⁺ T cell populations in Res vs NonRes

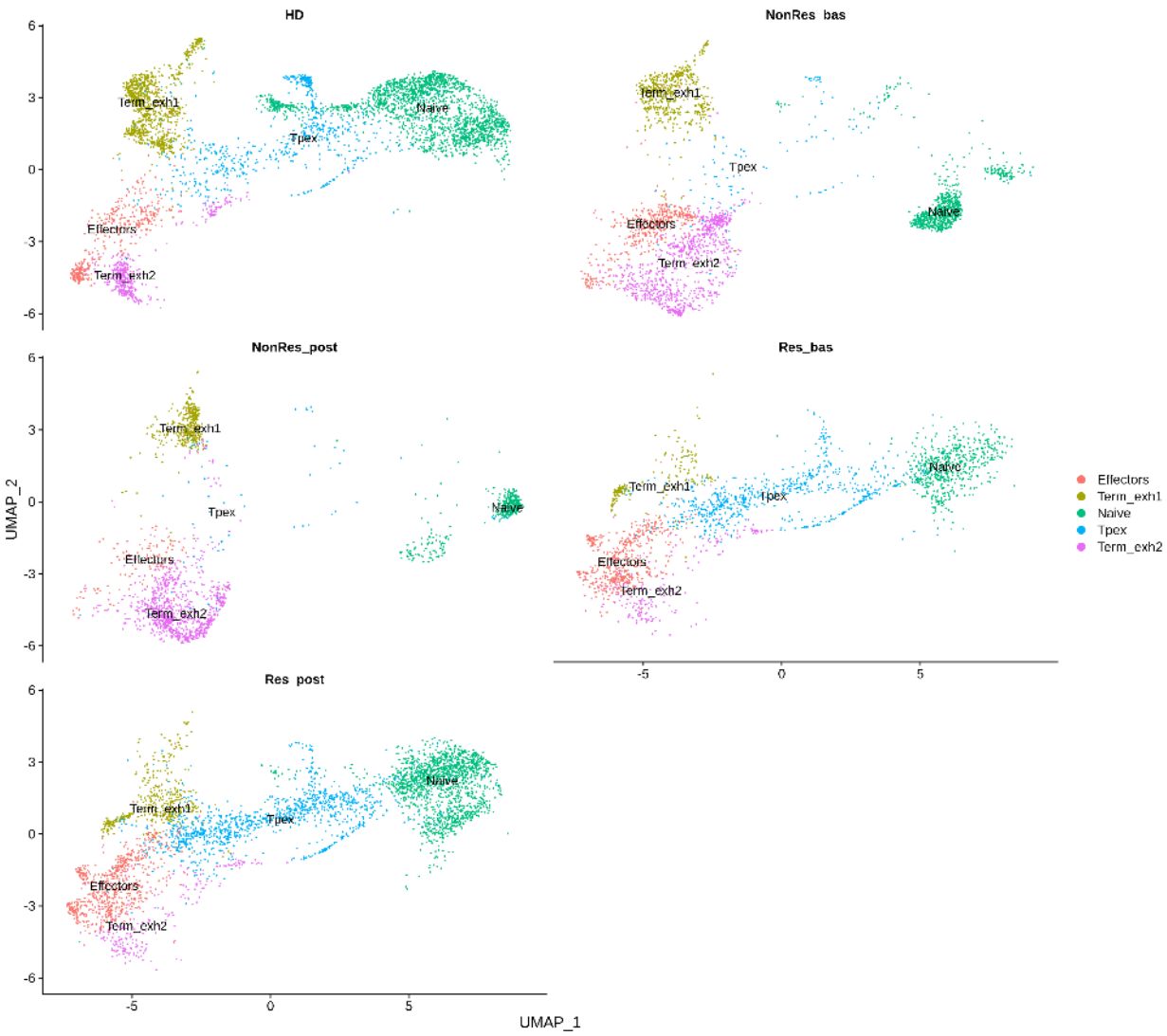

Figure 41: Res and NonRes have different cluster frequencies at both timepoints (baseline and post-treatment)

3.3 Tpex and Effectors are the most clonally expanded in Res whilst Term-exh2 are the most clonally expanded in NonRes

Based on these results, we hypothesized that Tpex and Effectors cells are putative functional subsets and may be predictive of response. To test this possibility, we measured the magnitude of clonal expansion in antigen experienced $CD8^+$ T cells in Res and NonRes by generating an overlay of the position of the most clonally expanded cells projected onto the 2D UMAP (Fig. 12A, B). The most clonally expanded subsets were Tpex and Effectors in Res and Term_exh2 in NonRes (Fig. 12A-C) revealing a strong relationship between frequencies and clonal expansion of the $CD8^+$ T-cell subsets.

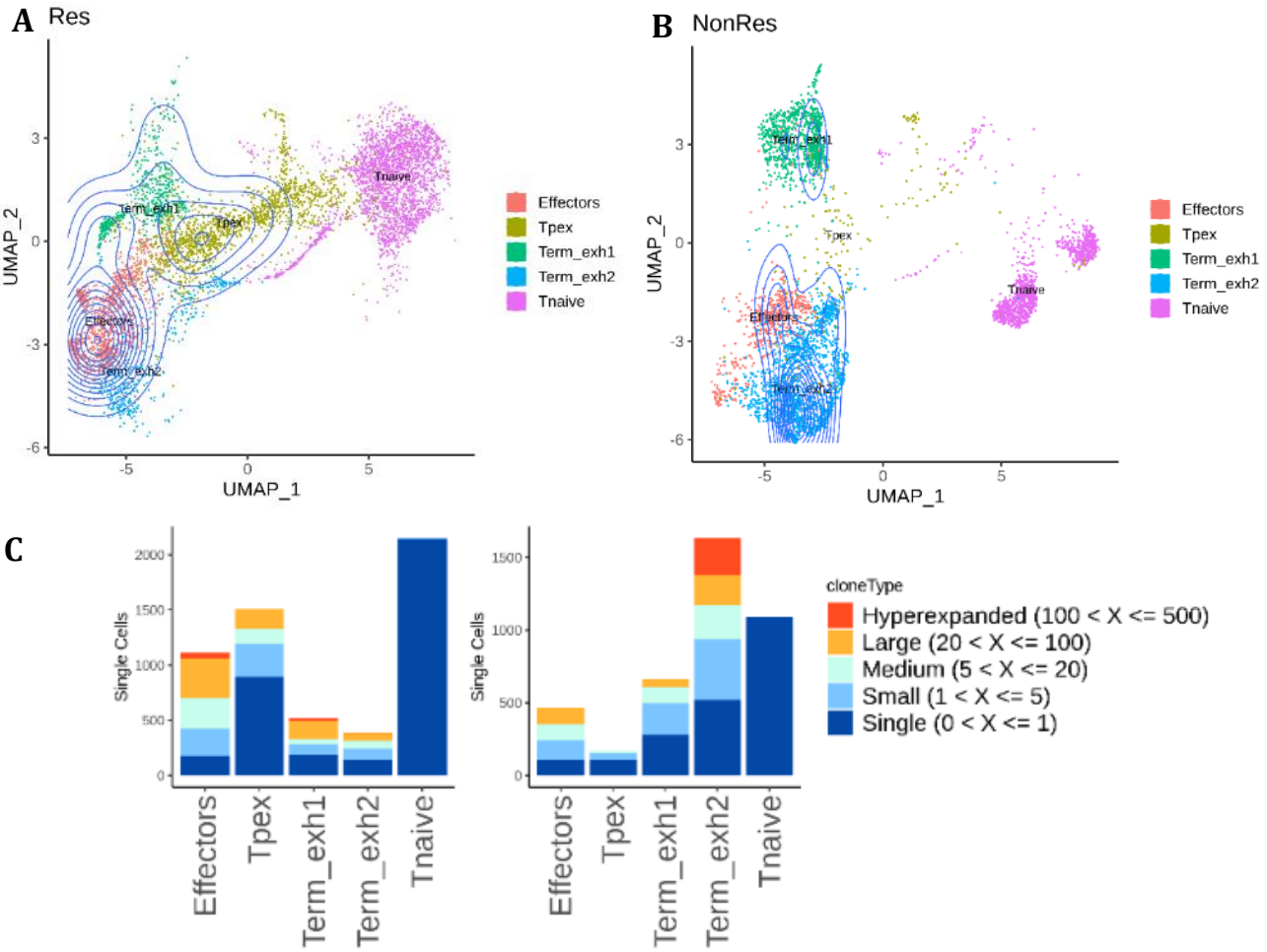

Figure 12: Tpex and effectors are the most clonally expanded in Res vs NonRes while Term_exh2 are most clonally expanded in NonRes vs Res
(A-B) Lineage relationships between T cell phenotypes and clones detected by scRNAseq and scTCRseq analysis. The contour plots show that Tpex and effectors in Res(A) and Term_exh2 in NonRes(B) are the most clonally expanded. (C) Stackplot showing the count of cells by cluster assigned into specific frequency ranges of clonotype

Collectively, these data identified $GZMK^+IL7R^+$ cells as a distinct entity in the early differentiated $CD8^+$ memory T cell pool and further showed that this subset is increased and clonally expanded in Res compared to NonRes.

3.4 $CD8^+$ $GZMK^+CD127^+$ progenitor exhausted cells correlate with response and overall survival

Building on the scRNAseq findings, we designed a 26-color spectral flow cytometry panel to explore T cell phenotypes at the protein level and analyzed 22 AML patients (12 Res and 10 NonRes) at baseline and post-chemotherapy. The single-marker evaluation revealed an increase of GZMK and CD127 at baseline in Res VS NonRes. TCF1, TIGIT and PD1 were also increased at baseline in Res. Hierarchical metaclustering of FlowSOM clusters identified $CD8^+$ $GZMK^+CD127^+$ T cells as a distinct memory $CD8^+$ subpopulation. This cluster, consistently with scRNAseq findings, was increased at baseline in Res VS NonRes (Fig 13 A-C). Remarkably, this cluster was characterized by the expression of TIGIT, PD1 and TCF-1. Of note, the only other cluster with a higher expression of TCF-1 was $CD8^+$ naive cells which are known to express high levels of this transcription factor (Zhao X *et al*, 2021).

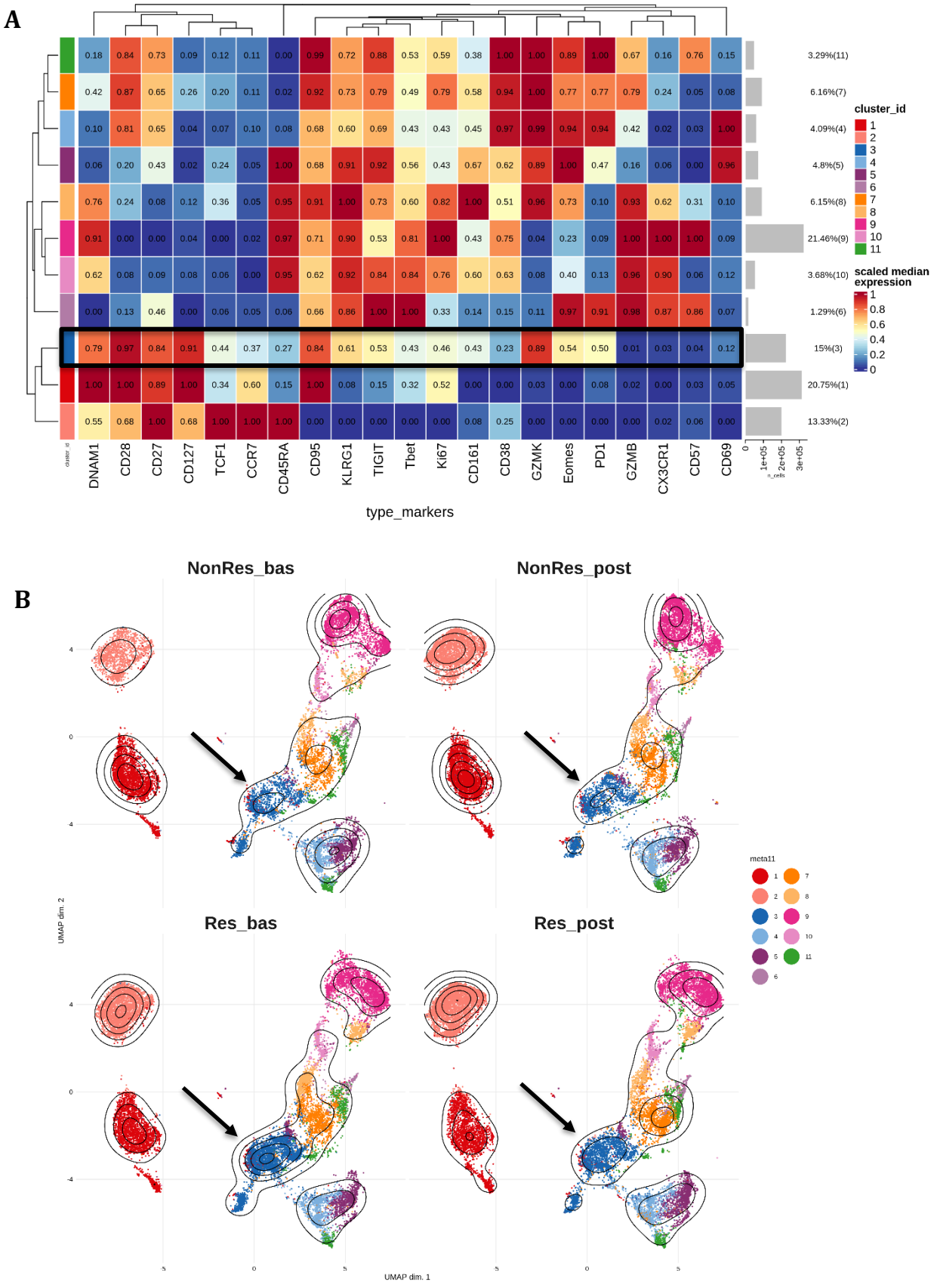
A
DNAM1
CD28
CD27
CD127
TCF1
CCR7
CD45RA
CD95
KLRG1
TIGIT
Tbet
Ki67
CD161
CD38
GZMK
Eomes
PD1
GZMB
CX3CR1
CD57
CD69
type_markers
3.29%(11)
6.16%(7)
4.09%(4)
4.8%(5)
6.15%(8)
21.46%(9)
3.68%(10)
1.29%(6)
15%(3)
20.75%(1)
13.33%(2)
cluster_id
scaled median expression
B
NonRes_bas
NonRes_post
Res_bas
Res_post
UMAP dim. 1
UMAP dim. 2
meta11

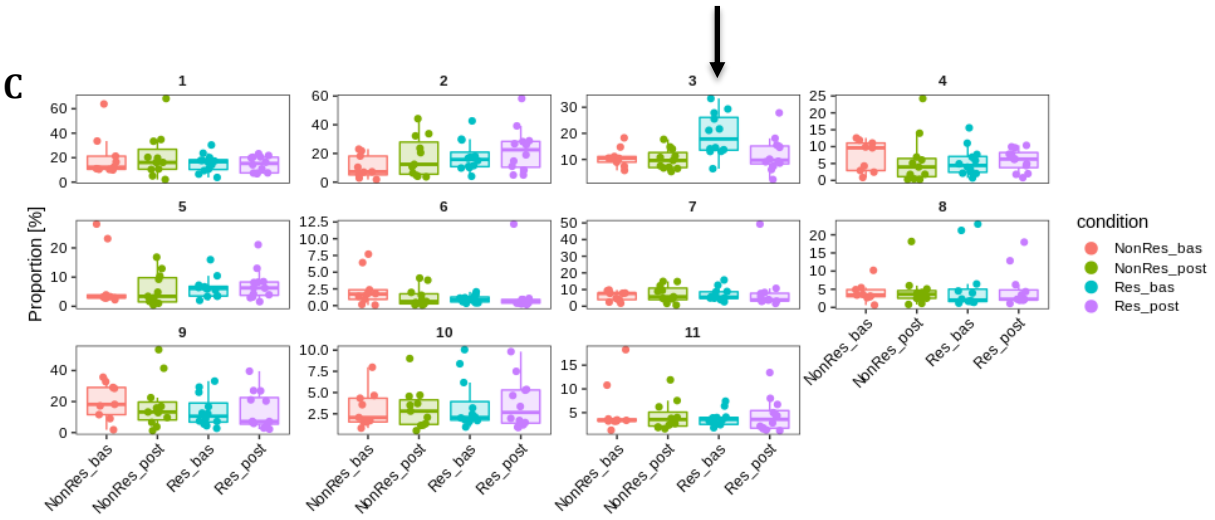

Figure 13: scRNAseq guided spectral flow-cytometry analysis confirms that BM GZMK⁺IL7R⁺ CD8⁺ T cells are increased in patients who are more likely to respond to chemotherapy

(A)Heatmap showing the 0-1 scaled MFI values of 21 markers over eleven CD8+ BM subsets from 22 AML patients (12 Res and 10 NonRes) at baseline and post-treatment. The median marker expression identifies the markers that drive each cell subset. Each CD8+ subpopulation is colored according to the cluster identified using the FlowSOM algorithm. GZMK+IL7R+CD8⁺ cluster highlighted. (B) UMAP visualization overlaid with contour plots (kernel density estimation) of the eleven CD8+ BM subpopulations in all the AML patients (Res, n = 12, NonRes, n = 10), at baseline and after therapy. Each CD8+ subpopulation is colored according to the cluster identified using the FlowSOM algorithm. (C) Boxplots showing the relative abundance of BM CD8+ subpopulations in NonRes and Res patients at baseline and post-treatment.

The results obtained with the FlowSOM algorithm were subsequently reproduced by standard flow cytometry gatings. Accordingly, manually gated GZMK$^+$CD127$^+$ CD8$^+$ T cells were significantly (**, $p < 0.01$) enriched in Res vs NonRes (Fig. 14 A, B). Furthermore, patients with a higher-than-median frequency of GZMK$^+$IL7R$^+$CD8$^+$ T cells experienced significantly (*, $p < 0.05$) longer overall survival after therapy (Fig. 14 C). Therefore, an increased abundancy of progenitor exhausted CD8$^+$ T cells in

the BM microenvironment is associated with chemotherapy efficacy and prolonged survival in patients with AML.

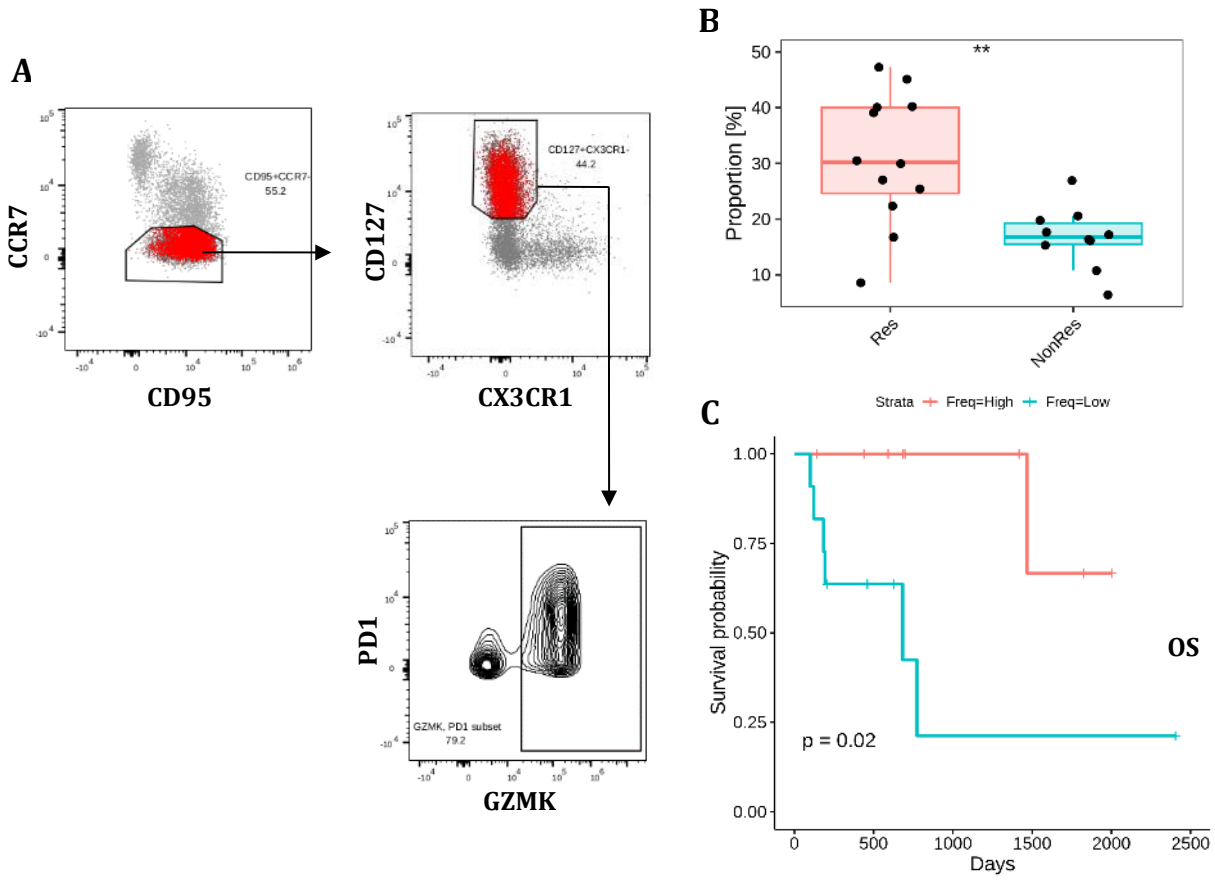

Figure 14: Manual gating confirms the enrichment of BM GZMK⁺IL7R⁺ CD8⁺ T cells and the advantage in OS in patients with high frequencies
(A) Gating strategy for GZMK⁺IL7R⁺ CD8⁺ T cells. (B) Boxplot showing the different frequency of GZMK⁺IL7R⁺ CD8⁺ T cells in Res and NonRes. Horizontal bars indicate median values. Asterisks indicate adjusted p-values (*padj< 0.05). (C) Kaplan-Meier estimate of OS: patients with a higher-than-median frequency of GZMK⁺IL7R⁺ CD8⁺ T cells experience significantly (*p< 0.05) prolonged OS after chemotherapy.

3.5 Exhaustion is a multistep process that broadly affects T cell differentiation during chronic antigen stimulation

Due to its nature, unsupervised clustering does not capture the phenotypic transition between the different transcriptional cell subsets. To achieve this, we used trajectory-inference methods and ordered the cells along the pseudotime (Slingshot) (Street et al., 2018) on our scRNAseq dataset. This analysis identified T-cell differentiation dynamics revealing that Tpex population splits into two branches representing two distinct developmental states where Term_exh1 (Lineage 1) and Term_exh2 (Lineage 2) are the terminal stages (Fig 15 A). Thus, Slingshot analysis suggests that upon antigen recognition in the BM, Tpex cells differentiate either into Term_exh1, present in all the subgroups (Res, NonRes, HDs) or into Term_exh2 which is almost exclusively present in NonRes.

To identify the drivers of the dichotomic differentiation trajectories, we studied the genes differentially expressed between the two lineages at the point of trajectory divergence. CD52 was among the most significant differentially expressed genes between the two lineages (Fig. 15 B). This gene was indeed highly expressed in Term_exh2, but not in Term_exh1 (Fig. 15 C). Given Term_exh2 being the end-stage of lineage 1 and given its increased frequency in NonRes, we hypothesized that these are the dysfunctional senescent cells already described to be increased at baseline and post-therapy in AML patients (Knaus HA *et al*, 2018).

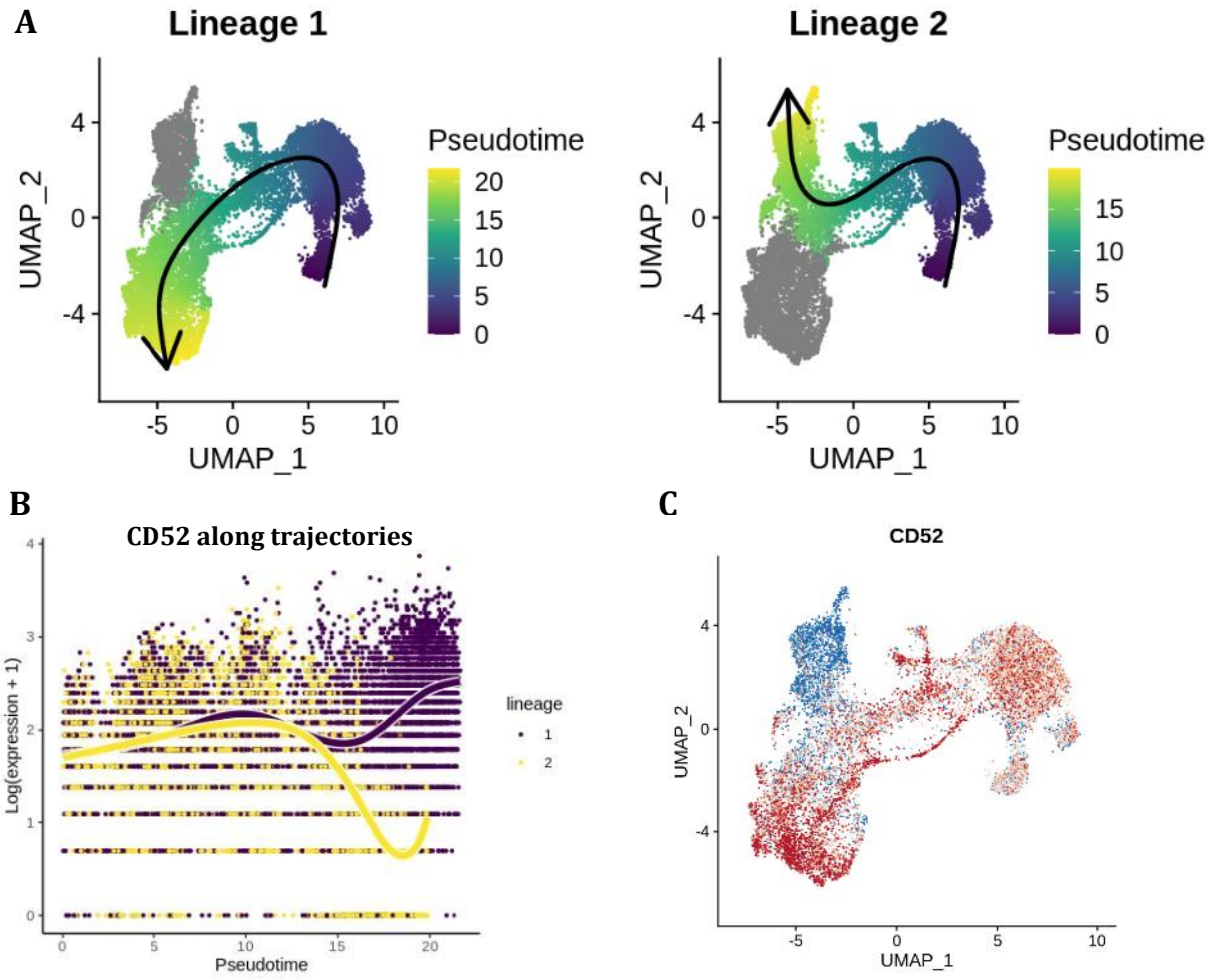

Figure 15: Trajectories showing a CD52 driven dichothomic differentiation of BM CD8⁺ T cells
(A) scRNAseq UMAP overlaid with slingshot-based cell trajectories starting at Tnaive and proceeding into Term_exh1 or Term_exh2. (B) Differential gene-expression between the two identified trajectories at the bifurcation identified CD52 as one of the drivers of the lineages' split. (C) CD52 is upregulated in Term_exh2, downregulated in Term_exh1

To support this hypothesis, we interrogated the TCGA-LAML cohort and found that patients with higher-than-median expression of CD52 had a significantly reduced OS (Fig. 16). A limitation of this analysis is that being based on bulk-RNAseq data is not possible to understand which BM subpopulations contribute the most in CD52 expression and consequently

survival. The anti-CD52 monoclonal antibody (Alemtuzumab) is commonly used in chronic lymphocytic leukemia and multiple sclerosis (MS). However, there is limited experience in the treatment of AML with anti-CD52 (Saito Y *et al*, 2011). Since CD52 is notoriously expressed in differentiated CD8+ T cells and Tregs, our data lay the bases for further in-depth analyses of the role of CD52 expression on T cells in AML. If confirmed anti-CD52 may inhibit Temra and Tregs favoring the persistence of potentially functional effectors.

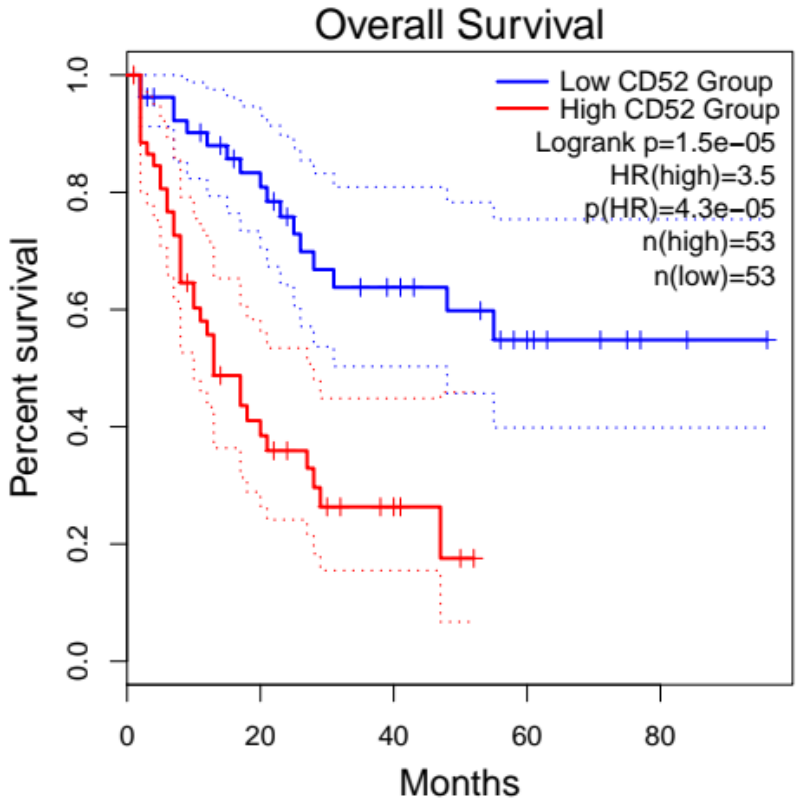

Figure 16: Higher-than-median CD52 expression is associated with survival advantage

4. Discussion

Tpex is a $CD8^+$ subpopulation present in tumor microenvironment that is polifunctional, has high proliferative potential and can differentiate in terminally exhausted $CD8^+$ T cells.

In this study, we identified BM T-cell subsets that correlate with response to chemotherapy in patients with AML. Others previously described these subpopulations but mainly in murine models and in solid tumors and chronic infections (Siddiqui *et al.*, 2019; Miller *et al.*, 2019; Beltra JC *et al.*, 2020) To the best of our knowledge, this is the first in-depth analysis of T cell dysfunction performed on human samples from AML patients.

Our data have several implications for understanding immune exhaustion in AML and its clinical relevance. First, we identified a T-cell subset that correlates with response to chemotherapy and to chemotherapy plus ICB. Second, we identified and characterized a subpopulation of Tpex which is clonally and transcriptionally distinct as well as differentially abundant in Res vs NonRes to chemotherapy. Remarkably, the frequency of this subpopulation at baseline predicts overall survival. Further in vitro and in vivo analyses may help clarify the proliferation potential, antigen specificity and functionality of this subset in AML. Third, we identified a subset of terminally exhausted/senescent $CD8^+$ T cells (Term_exh2) to be increased and clonally expanded in NonRes vs Res already at diagnosis. As expected, this subpopulation expresses markers of cytotoxicity and is located at the end of the developmental trajectory. These findings suggest that both Tpex and senescent $CD8^+$ cells could potentially be used as biomarkers to identify patients that are at increased risk of early relapse after chemotherapy. The identification of the defining markers of these subsets is critical to design

broadly applicable diagnostic panels to better stratify AML risk and, therefore, guide treatment decisions.

Furthermore, our unbiased approach confirmed that Tpex in AML have a stem-like transcriptional signature. Therefore, the in-depth characterization of this subset will likely play a role in overcoming some of the obstacles of T-cell therapies in AML. Finally, our data indicate CD52 as a new potential marker of $CD8^+$ senescent cells in AML. Consistent with this, CD52 level of expression predicts survival in a TCGA cohort. If confirmed, these preliminary data would have a potential impact on the use of targeted treatments to reduce senescence and maintain functional antitumor $CD8^+$ T cells.

5 Tables

Table 1 Patients characteristics (Chemotherapy cohort – exploratory flow-cytometry)

Patients characteristics	**N = 16**
Age, median (range)	57.5 (26 - 76)
Male	9 (56%)
Female	7 (44%)
BM blast % prior to treatment, median (range)	72 (6-95)
NPM1 mutated	5 (31%)
FLT3 ITD	5 (31%)
IDH1	2 (13%)
c-KIT	2 (13%)
Healthy donors	**N = 12**
Age, median (range)	40 (27 - 50)

Table 2 Patients characteristics (HIDAC/Pembrolizumab cohort)

Patients characteristics	**N = 19**
Age, median (range)	54 (24 - 66)
Male	10 (52%)
Female	9 (48%)
BM blast % prior to treatment, median (range)	25 (6-89)
Relapsed AML	10 (52%)
Refractory AML	9 (48%)
NPM1 mutated	5 (26%)
FLT3 ITD	4 (21%)
DNMT3A mutated	3 (16%)
NRAS mutated	3 (16%)
ASXL1 mutated	2 (11%)
TP53 mutated	2 (11%)
RUNX1 mutated	2 (11%)

Table 3 Patients characteristics (Chemotherapy cohort – spectral flow-cytometry)

Patients characteristics	N = 22
Age, median (range)	56(26 – 74)
Male	13 (59%)
Female	9 (41%)
BM blast % prior to treatment, median (range)	68.5 (12-95)
NPM1 mutated	6 (27%)
FLT3 ITD	6 (27%)
NRAS mutated	3 (14%)
ASXL1 mutated	3 (14%)
DNMT3A mutated	2 (9%)
RUNX1 mutated	2 (9%)

Table 4 Flow-cytometry panel (Chemotherapy cohort – exploratory flow-cytometry)

Marker	Fluorochrome	Clone	Company	Cat #
CD3	BV510	OKT3	BioLegend	317332
CD8	BUV805	SK3	BD	564910
CD4	BUV805	SK1	BD	564912
CD56	BV786	5.1H11	BioLegend	362550
CD45RA	BUV395	HI100	BD	740298
CCR7	FITC	150503	BD	561271
CD27	AF700	O323	BioLegend	302814
CD28	BV650	CD28.2	BioLegend	302946
DNAM1	BV711	11A8	BioLegend	338334
CD57	Pacific Blue	QA17A04	BioLegend	393326
KLRG1	APC	2F1/KLRG1	BioLegend	138412
PD1	PE	EH12.1	BD	560795
Tim 3	PE-TR	F38-2E2	BioLegend	345034
CD69	BUV395	4B4-1	BD	745737

Table 5 Flow-cytometry panel (HIDAC/Pembrolizumab cohort)

Marker	Fluorochrome	Clone	Company	Cat #
CD3	BV605	OKT3	Biolrgend	317322
CD8	PerCPCy5.5	RPA-T8	e-Bioscience	45-0088-42
CCR7	BV650	G043H7	Biolegend	353234
CD45RA	APCCy7	HI100	BioLegend	304128
CD56	PECF594	B159	BD	562289
CD28	PECy7	CD28.2	e-Bioscience	25-0289-42
CD57	V450	HCD57	BioLegend	322316
CD27	AF700	M-T271	BD	560611
PD1	PE	EH12.1	BD	560795
KLRG1	APC	SA231A2	BioLegend	367716
CD160	AF488	BY55	eBioscience	53-1609-42
BTLA	AF647	MIH26	BioLegend	344510
2B4	FITC	C1.7	BioLegend	329506
Tim3	PE	FAB2365P	R & D	344823
CD95	ef450/pacblue	DX2	Biolegend	305619

Table 6 Flow-cytometry panel (Chemotherapy cohors – spectral flow-cytometry)

Marker	Fluorochrome	Clone	Company	Cat#
CD28	BB515	CD28.2	BD Biosciences	564492
CCR7	PB	G043H7	BioLegend	353210
CD3	APC-Fire750	UCHT1	BioLegend	300470
CD38	APC/Fire810	HIT2	BioLegend	303550
CD4	Spark NIR685	SK3	BioLegend	344658
CD57	BV510	QA17A04	BioLegend	393314
CD95	BV650	DX29	BioLegend	305642
DNAM1	BV785	11A8	BioLegend	338322
PD1	PE/Dazzle594	EH12.2H7	BioLegend	329940
Tbet	KB520	4B10	BioLegend	644838
TIGIT	BV421	A15153G	BioLegend	372710
Viability	Zombie NIR	n/a	BioLegend	423106
CD45RA	BV570	HI100	BioLegend	304132
CD27	BV605	O323	BioLegend	302830
CD8	AlexaFluor 532	RPA-T8	eBiosciences	58-0088-42
Eomes	PE-Cy7	WD1928	eBiosciences	25-4877-42
KLRG1	PerCP-eFluor 710	13F12F2	eBiosciences	46-9488-42
CX3CR1	BV750	2A9-1	BDBiosciences	747376
CD161	BB700	DX12	BDBiosciences	745791
Ki67	BV480	B56	BDBiosciences	566109
CD127	BV711	A019D5	BioLegend	351328
TCF1	PE	C63D9	CellSignalingTechnology	14456S
CD69	PE-Cy5	FN50	BioLegend	310908
GZMK	AlexaFluor 647	GM6C3	SantaCruz	AF647
GZMB	AlexaFluor 700	GB11	BDBiosciences	560213
CD33	SB436	P67.6	eBiosciences	62-0337-42
CD117	SB436	104D2	eBiosciences	62-1178-42

6 Acknowledgements

It is a great pleasure to express my full gratitude to Professor Leo Luznik. Our collaboration started remotely, three years ago, talking of science and leukemia. After one year he accepted to let me join his lab. Since then his dedication and attitude to help have allowed me to grow as a scientist. I owe him the chance to work in a stimulating environment at Johns Hopkins; for this reason my biggest thank is to him. This work wouldn't have been possible without my lab fellows Rupkatha Mukhopadhyay and Anish Chowdhury who have helped me with timely advices.

Luca Biavati, friend and colleague, supported me throughout my period at Johns Hopkins. His expertise as a doctor and researcher helped me to think and develop this work.

Thanks to Ivan Borrello and his team for their help and for letting me use their instruments.

Thanks to my family for the never ending support.

Thanks to my friends Luca, Cristina and Francesco in Baltimore. Special thanks go to Kat for her invaluable support. Thanks to Sonali for her friendship and guidance during the last years.

Thanks to Marco, Pasquale, Alessandro, Angela, Stelios and Marzia. Thanks to my old fellow and friend Lorenzo.

Thanks to the Hematology Division of University of Pisa. In particular thanks to Professor Mario Petrini, my first mentor, for his support and

thoughtful suggestions. He helped me to become a doctor and to develop my skills as a scientist.
Special thanks to Nadia Cecconi, Francesco Caracciolo, Giulia Cervetti, Rita Fazzi, Enrico Orciuolo, Gabriele Buda, Giancarlo Carulli, Matteo Pelosini, Claudia Barate', Giovanni Consani for helping me to become a clinician.
Thanks to Professor Sara Galimberti for her support and supervision as a fellow first and as a PhD student later on. Thanks to all the member of the lab in Pisa. Special thanks to Simone Pacini and Marina Montali who started helping me with my first experiments as a graduate. Thanks to Paola Sammuri, Elena Ciabatti, Susanna Grassi, Francesca Guerrini and Serena Salezadeh.

Rotary International has given unconditional support for my stay in the US with a Global Scolarship.

References

1. Liersch R, Müller-Tidow C, Berdel WE , et al. Prognostic factors for acute myeloid leukaemia in adults–biological significance and clinical use. *Br J Haematol* 165, 17-38 (2014).

2. Walter RB, Pagel JM, Gooley TA, et al. Comparison of matched unrelated and matched related donor myeloablative hematopoietic cell transplantation for adults with acute myeloid leukemia in first remission. *Leukemia* 24, 1276-82 (2010).

3. Burnett AK, Goldstone A, Hills RK, et al. Curability of patients with acute myeloid leukemia who did not undergo transplantation in first remission. *J Clin Oncol* 31, 1293-301 (2013).

4. Grimwade D, Walker H, Oliver F, et al. The importance of diagnostic cytogenetics on outcome in AML: analysis of 1,612 patients entered into the MRC AML 10 trial. The Medical Research Council Adult and Children's Leukaemia Working Parties. *Blood* 92, 2322-33 (1998).

5. Döhner H, Estey E, Grimwade E, et al. Diagnosis and management of AML in adults: 2017 ELN recommendations from an international expert panel. *Blood* 129, 424-447 (2017).

6. Schuurhuis GJ, Heuser M, Freeman S, et al. Minimal/measurable residual disease in AML: a consensus document from the European LeukemiaNet MRD Working Party. *Blood* **131**, 1275-1291 (2018).

7. Weiden PL, Sullivan KM, Flournoy N, et al. Antileukemic effect of chronic graft-versus-host disease: contribution to improved survival after allogeneic marrow transplantation. *N Engl J Med* 304, 1529-33 (1981).

8. Parmar S, Fernandez-Vina M, De Lima M. Novel transplant strategies for generating graft-versus-leukemia effect in acute myeloid leukemia. *Curr Opin Hematol* 18, 98-104 (2011).

9. Kanakry, C., Fuchs, E. & Luznik, L. Modern approaches to HLA-haploidentical blood or marrow transplantation. Nat Rev Clin Oncol 13, 10–24 (2016).

10. Ringdén O, Boumendil A, Labopin M, et al. Outcome of Allogeneic Hematopoietic Stem Cell Transplantation in Patients Age >69 Years with Acute Myelogenous Leukemia: On Behalf of the Acute Leukemia Working Party of the European Society for Blood and Marrow Transplantation. *Biol Blood Marrow Transplant* 25, 1975-1983 (2019).

11. Daver N, Alotaibi AS, Bücklein V, et al. T-cell-based immunotherapy of acute myeloid leukemia: current concepts and future developments. *Leukemia* 35**,** 1843–1863 (2021).

12. Qasim W. Allogeneic CAR T cell therapies for leukemia. American journal of hematology 2019;94:S50-4.

13. Chapuis AG, Thompson JA, Margolin KA, et al. Transferred melanoma-specific CD8+ T cells persist, mediate tumor regression, and acquire central memory phenotype. Proc Natl Acad Sci USA 2012;109:4592–4597.

14. Maude SL, Frey N, Shaw PA, et al. Chimeric antigen receptor T cells for sustained remissions in leukemia. *N Engl J Med*. 2014;371(16):1507–1517.

15. Youngblood B, Davis CW, Ahmed R. Making memories that last a lifetime: heritable functions of self-renewing memory CD8 T cells. *Int. Immunol.* 22, 797–803 (2010).

16. Wherry EJ, Kurachi M. Molecular and cellular insights into T cell exhaustion. *Nat. Rev. Immunol.* **15**, 486–499 (2015).

17. Long AH, Haso WM, Shern JF et al. 4-1BB costimulation ameliorates T cell exhaustion induced by tonic signaling of chimeric antigen receptors. *Nat Med*. 2015;21(6):581–590.

18. Sharpe A, Pauken K. The diverse functions of the PD1 inhibitory pathway. *Nat Rev Immunol* 18**,** 153–167 (2018).

19. Robert C., Schachter J, Long GV et al. Pembrolizumab versus ipilimumab in advanced melanoma. *N. Engl. J. Med.* 372, 2521–2532 (2015).

20. Larkin J, Chiarion-Sileni V, Gonzalez R et al. Five-year survival with combined nivolumab and ipilimumab in advanced melanoma. N. Engl. J. Med. N Engl J Med 2019; 381:1535-1546 (2019).

21. Ansell SM, Lesokhin AM, Borrello I, et al. PD-1 blockade with nivolumab in relapsed or refractory Hodgkin's lymphoma. N Engl J Med 372:311-319, 2015

22. Khan O, Giles JR, McDonald S, et al. TOX transcriptionally and epigenetically programs CD8+ T cell exhaustion. *Nature* **571**, 211-218 (2019).

23. Muroyama Y, Wherry EJ. Memory T-Cell Heterogeneity and Terminology. Cold Spring Harb Perspect Biol. 2021.

24. Beltra JC, Manne S, Abdel-Hakeem MS, et al. Developmental Relationships of Four Exhausted CD8 + T Cell Subsets Reveals Underlying Transcriptional and Epigenetic Landscape Control Mechanisms. Immunity 52, 825–841, May 19, 2020

25. Chen, Z, Ji, Z, Ngiow SF, et al. TCF-1-Centered Transcriptional Network Drives an Effector versus Exhausted CD8 T Cell-Fate Decision. Immunity 51, 840–855.e5, e845 (2019).

26. McLane LM, Abdel-Hakeem M S, Wherry EJ. CD8 T cell exhaustion during chronic viral infection and cancer. Annu. Rev. Immunol. 37, 457–495 (2019).

27. Siddiqui I, Schaeuble K, Chennupati V, et al. Intratumoral Tcf1+PD-1+CD8+T cells with stem-like properties promote tumor control in response to vaccination and checkpoint blockade immunotherapy. Immunity 50, 195–211.e10 (2019).

28. Abdel-Hakeem MS, Manne S, Beltra, JC. et al. Epigenetic scarring of exhausted T cells hinders memory differentiation upon eliminating chronic antigenic stimulation. Nat Immunol 22, 1008–1019 (2021). https://doi.org/10.1038/s41590-021-00975-5

29. Galletti G, De Simone G, Mazza EMC, et al. Two subsets of stem-like CD8+ memory T cell progenitors with distinct fate commitments in humans. *Nat Immunol* 21, 1552-1562 (2020).

30. Reiser, J. & Banerjee, A. Effector, memory, and dysfunctional CD8(+) T cell fates in the antitumor immune response. *J. Immunol. Res.* 2016, 8941260 (2016).

31. Akbar, A. N. & Henson, S. M. Are senescence and exhaustion intertwined or unrelated processes that compromise immunity? Nat. Rev. Immunol.11, 289–295 (2011).

32. Liu, X. et al. Regulatory T cells trigger effector T cell DNA damage and senescence caused by metabolic competition. Nat. Commun.9, 249 (2018).

33. Vago L, Gojo I. Immune escape and immunotherapy of acute myeloid leukemia. *J Clin Invest.* 2020;130(4):1552-1564.

34. Szczepanski MJ, Szajnik M, Czystowska M, et al. Increased frequency and suppression by regulatory T cells in patients with acute myelogenous leukemia. *Clin Cancer Res* 15, 3325-32 (2009).

35. Buggins AG, Milojkovic D, Arno MJ, et al. Microenvironment produced by acute myeloid leukemia cells prevents T cell activation and proliferation by inhibition of NF-kappaB, c-Myc, and pRb pathways. *J Immunol* 167, 6021-30 (2001).

36. Al-Matary YS, Botezatu L, Opalka B, et al. Acute myeloid leukemia cells polarize macrophages towards a leukemia supporting state in a Growth factor independence 1 dependent manner. *Haematologica* 101, 1216-1227 (2016).

37. Nowicka M, Krieg C, Crowell HL, et al. CyTOF workflow: differential discovery in high-throughput high-dimensional cytometry datasets. *F1000Res* **6**, 748 (2017).

38. Weber LM, Nowicka M, Soneson C, et al. diffcyt: Differential discovery in high-dimensional cytometry via high-resolution clustering. *Commun Biol* 2, 183 (2019).

39. Lun ATL, Riesenfeld S, Andrews T, et al. EmptyDrops: distinguishing cells from empty droplets in droplet-based single-cell RNA sequencing data. *Genome Biol* 20, 63 (2019).

40. Bais AS, Kostka D. scds: computational annotation of doublets in single-cell RNA sequencing data. *Bioinformatics* 36, 1150-1158 (2020).

41. McCarthy DJ, Campbell KR, Lun AT,. Scater: pre-processing, quality control, normalization and visualization of single-cell RNA-seq data in R. *Bioinformatics* 33, 1179-1186 (2017).

42. Stuart T, Butler A, Hoffman P, et al. Comprehensive Integration of Single-Cell Data. *Cell* 177, 1888-1902.e21 (2019).

43. Butler A, Hoffman P, Smibert P, et al. Integrating single-cell transcriptomic data across different conditions, technologies, and species. *Nat Biotechnol* 36, 411-420 (2018).

44. Borcherding N, Bormann NL, Kraus G. scRepertoire: An R-based toolkit for single-cell immune receptor analysis. *F1000Res* 9, 47 (2020).

45. Jansen, C.S., Prokhnevska, N., Master, V.A. et al. An intra-tumoral niche maintains and differentiates stem-like CD8 T cells. Nature 576, 465–470 (2019).

46. Miller BC, Sen DR, Al AR, et al. Subsets of exhausted CD8+ T cells differentially mediate tumor control and respond to checkpoint blockade. *Nat Immunol* 20, 1556 (2019).

47. Dufva O, Pölönen P, Brück O, et al. Immunogenomic Landscape of Hematological Malignancies. *Cancer Cell* 38, 424-428 (2020).

48. Szabo PA, Levitin HM, Miron M, et al. Single-cell transcriptomics of human T cells reveals tissue and activation signatures in health and disease. Nat. Commun. 10, 4706 (2019).

49. Pace L, Goudot C, Zueva E, et al. The epigenetic control of stemness in CD8+ T cell fate commitment. Science 359, 177–186 (2018).

50. Zhao, X, Shan Q, Xue HH. TCF1 in T cell immunity: a broadened frontier. Nat Rev Immunol (2021).

51. Street K, Risso D, Fletcher RB, et al. Slingshot: cell lineage and pseudotime inference for single-cell transcriptomics. *BMC Genomics* 19, 477 (2018).

52. Hanna A. Knaus, Sofia Berglund, Hubert HacklHanna A. Knaus Knaus HA, Berglund S, Hackl H. Signatures of CD8+ T cell dysfunction in AML patients and their reversibility with response to chemotherapy. JCI Insight. 2018;3(21):e120974.

53. Saito Y, Nakahata S, Yamakawa N, Kaneda K, Ichihara E, Suekane A, Morishita K. CD52 as a molecular target for immunotherapy to treat acute myeloid leukemia with high EVI1 expression. Leukemia. 2011 Jun;25(6):921-31.